

pubs.acs.org/JPCC Article

Tailored Colloidal Nanostars for Surface-Enhanced Raman Spectroscopy: Optimization of Formulation Components and Study of the Stabilizer—Nanoparticle Interactions

Chiara Deriu, Asier Bracho, and Bruce McCord*



Cite This: J. Phys. Chem. C 2022, 126, 2023–2040



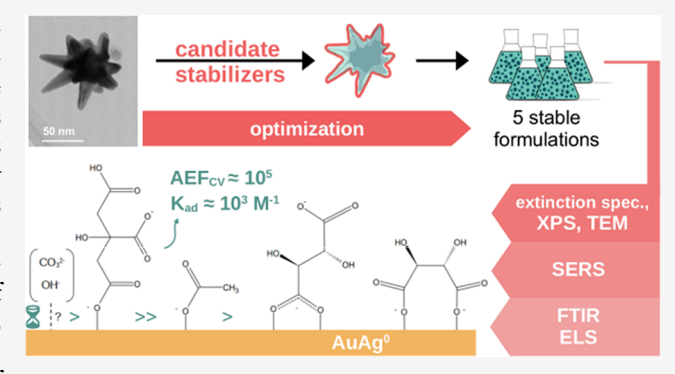
ACCESS I

Metrics & More

Article Recommendations

s Supporting Information

ABSTRACT: While the effects of the morphology and composition of plasmonic substrates in Surface-Enhanced Raman Spectroscopy (SERS) are widely studied, surface chemistry and, more specifically, the role of preadsorbed species on colloidal substrates (i.e., stabilizers and synthesis byproducts) are typically less explored. In this paper, a surfactant-free synthesis of sparingly capped bimetallic colloidal AuAg nanostars was selected as a basis to (1) examine the effect of varying stabilizers and (2) systematically assess the impact of the resulting surface environment on SERS intensity. The latter entailed the characterization of the colloidal formulations in terms of optical reproducibility, suitability for analytical applications, long-term colloidal stability, and SERS performance. Emphasis was given to the elucidation of



the stabilizer—metal interactions, which were studied by electrophoretic light scattering and infrared spectroscopy. It was found that the capping process is the result of chemisorption to an essentially neutral alloy and that the capping environment has effects on the SERS response that can overtop those caused by nanoparticle morphology. The model stabilizer, citrate, was found to weakly chemisorb $(-4.36 \pm 0.08 \text{ and } -4.58 \pm 0.05 \text{ kJ/mol}$ at 10 and 20 °C, respectively) to the bimetallic surface in a positively cooperative fashion $(n_{\text{Hill}} > 1)$ via the unidentate mode.

1. INTRODUCTION

Surface-Enhanced Raman Spectroscopy (SERS) is a surface spectroscopic technique in which the excitation of the localized surface plasmon resonance (LSPR) of a nanostructured substrate amplifies the inherently weak Raman signal of an adsorbed analyte by several orders of magnitude, up to and including single-molecule sensitivity. 1-5 The origin of the SERS phenomenon is plasmonic in nature, and consequently, an analyte's SERS signal is strongly dependent on its distance from the plasmonic surface. This requirement for substrate-analyte proximity raises the issue of dealing with surface interaction phenomena and in particular with adsorption. The adsorption behavior that a molecule exhibits when approaching a surface is dependent on the interplay of the association constants existing between the analyte molecules themselves and between the analyte molecules and the surface, which can be schematized in the following equilibria

$$A + A \stackrel{K_{AA}}{\Longrightarrow} [AA] \tag{1}$$

$$A + S \stackrel{K_{AS}}{\Longrightarrow} [AS] \tag{2}$$

where A is the analyte or adsorbate, S is the surface, and $K_{\rm AA}$ and $K_{\rm AS}$ are the equilibrium constants toward the formation of complexes.

Colloidal sols are the most popular type of enhancing substrate for SERS. When considering colloidal sols in terms of the adsorption equilibria in eqs 1 and 2, it must be recalled that their surfaces cannot exist as chemically bare entities^{7–9} and will naturally have a population of adsorbed species on them. Therefore, there are always more than two association constants that need to be considered when carrying out SERS measurements in colloidal sols. In fact, several equilibria are established, not only between analyte molecules and between the analyte and surface (eqs 1 and 2) but also between capping species (C_1 , C_2 , ..., C_i) and surface ($K_{C,A}$).

Received: September 15, 2021 Revised: December 28, 2021 Published: January 25, 2022





$$C_i + S \stackrel{K_{C_iS}}{\Longrightarrow} [C_iS] \tag{3}$$

$$C_i + A \xrightarrow{K_{C_i A}} [C_i A] \tag{4}$$

Because SERS is a plasmonic, near-field effect, optimal conditions for signal production and consequent low limits of detection will be achieved not only when suitable preresonance conditions¹⁰ between the substrate and excitation source are met but also when equilibrium constants in the systems are conducive to analyte adsorption on the substrate. A strongly interacting analyte will be detectable at lower concentrations than a weaker one, their polarizabilities being similar. Therefore, when designing and optimizing a SERS colloidal substrate, it is important to consider the chemical environment at the solid/liquid interface of the nanoparticle¹¹ and the energies governing it.

While multiple studies have been published on the effects of morphology and composition of plasmonic nanostructures and their relationships with excitation wavelength, 10,12-19 significantly less work has been done on the effect of capping agents on colloidal sols (e.g., stabilizers and synthesis byproducts), their adsorption modes, and their effect on SERS performance. The literature on the surface chemistry of the SERS environment mostly entails the modification of the surface of colloidal sols during sample preparation, such as changing the pH of the sol²⁰ or removing excess surfactant species by centrifugation, 17 with the ultimate aim of forcing the analyte to adsorb on the surface. 11 On the other hand, a systematic study of the interactions between the capping agents and metal nanoparticles is much less explored. Most of the work on this topic has been performed outside of the SERS field and predominantly focuses on the elucidation of the adsorption modes of citrate on traditional gold colloidal nanoparticles. For example, Al-Johani et al.²¹ extensively characterized the surface of borohydride-reduced citrate-capped gold nanospheres, utilizing a wide range of analytical techniques, such as X-ray photoelectron spectroscopy (XPS) and multiple-quantum magic-angle spinning (MQMAS) and solid-state nuclear magnetic resonance (NMR), to determine the oxidation state of the metal surface and the binding mode of citrate. Their results indicated that citrate is chemisorbed to an essentially neutral gold surface via coordinating covalent bonding and that the specific coordination motif depends on surface coverage. Park and Shumaker-Parry²² studied the capping crown of citrate-reduced gold nanospheres by infrared (IR) spectroscopy and proposed instead a multi-layer citrate network model held by hydrogen bonds and van der Waals forces, concluding that there was no chemisorption on the metallic surface driving the formation of the capping layer. Although the nanoparticle systems studied by Al-Johani et al.²¹ and Park and Shumaker-Parry²² are different from each other (borohydride reduction followed by citrate capping vs citrate reduction and capping), the two publications are instrumental to the introduction of another critical point in the elucidation of the interactions between the plasmonic surface and capping agents, that is, there is no consensus on the oxidation state of the surface metal of the nanoparticle. More specifically, there is no consensus on whether chemical (i.e., covalent or coordinating covalent) or electrostatic adsorption is the actual driving cause of the capping process itself.

Determining whether covalent or electrostatic adsorption occurs between the metal substrate and capping species is

particularly important when considering eqs 3 and 4. Because the strength of the interaction between a substrate and a covalently adsorbed species would be different from that of an electrostatically adsorbed species, their respective equilibrium constants would also be different. Consequently, the presence of a capping agent on the surface may interfere with analyte—metal interactions, such as increasing the distance between the analyte and surface, thus affecting the intensity of the SERS signal. Ultimately, a rationally designed colloidal substrate should have capping species (i.e., stabilizers) that are able to both reside at the solid/liquid interface and provide stability and be easily displaceable by the analyte of interest.

As previously mentioned, SERS-focused work on the relationship between capping species and analytes is scarce and is mostly ascribable to the research efforts of Haes' group on nanoparticle stability. ^{23–26} In a recent publication, ²⁶ they studied the role of 4-(2-hydroxyethyl)-1-piperazineethanesulfonic acid (HEPES) in the SERS detection of benzene, utilizing HEPES-reduced and stabilized gold nanostars. ²⁷ The affinity of HEPES for the gold surface of the nanostars was demonstrated to be a function of pH; the changes in the electron distribution that HEPES undergoes under acidic conditions were observed to decrease the strength of the interaction with the surface, allowing their analyte, benzene, to adsorb and be detected by SERS. This study highlights the importance of interactions between the surface and stabilizer and their role in enabling analyte detection.

In the present study, a set of SERS-active colloidal bimetallic nanostars was utilized to develop a better understanding of the adsorption of stabilizers onto the nanoparticle surface and the resultant interplay between colloidal stability and SERS performance. The goal for these studies was to provide guidance on the development of SERS-based detection protocols through the use of surface chemistry. The platform that was chosen for this work was the bimetallic AuAg colloidal nanostars first synthesized by Cheng et al.²⁸ and later refined by He et al.¹⁷ for use as a SERS substrate. The synthesis makes use of L-ascorbic acid (L-AA) as the reducing agent, aurochloric acid as the precursor of the main metal constituent, and silver nitrate as the shape director. 17,28 The advantage of this nanofabrication protocol is that a systematic optimization of synthetic parameters with respect to SERS performance has already been conducted.¹⁷ The selected molar ratios (Au/L-AA = 3.5) for the present research were those reported by He et al.¹⁷ to provide the highest SERS enhancements at an excitation wavelength of 785 nm; this corresponds to the longest branch length and the most uniform spike density (Au/ Ag = 18:1).

Another advantage is that this synthesis results in colloidal nanostars that have a relatively low surface coverage by charged species (Supporting Information). As a result, optimal electrostatic repulsions between individual nanoparticles are not achieved, causing the sol to irreversibly aggregate ^{29,30} soon after synthesis. This instability was offset by Cheng et al. ²⁸ via the post-synthetic addition of the polymer *O*-carboxymethylchitosan, while He et al. ¹⁷ replaced the polymer with the surfactant cetyltrimethylammonium bromide (CTAB). As noted by the authors themselves, ¹⁷ bulky capping agents like CTAB give rise to SERS signal loss and higher limits of detection. ¹¹ An ideal SERS-compatible stabilizer should increase the shelf life of the colloidal formulation without interfering with the SERS signal production. Thus, our goal in this project was to modify the abovementioned colloidal

formulations through the application of alternative postsynthetic capping agents and then examine their effects on surface chemistry, colloid stability, and SERS response.

The present paper is organized into three parts. The first part presents the development of alternatively stabilized AuAg nanostar formulations. The selection of the initial array of candidate stabilizers was based on DLVO theory, ^{29,31-34} and the selection and refinement of the colloidal formulations were achieved using extinction spectroscopy and electrophoretic light scattering (ELS). Next, in the second part of this work, the obtained formulations were characterized in terms of reproducibility, suitability for analytical applications, long-term colloidal stability, and SERS performance using the ideal SERS probe crystal violet (CV). The importance of the surface environment was also examined utilizing fentanyl analogs as nonideal SERS probes. Finally, the third part of this work characterizes the stabilizer-metal interaction utilizing ELS and IR spectroscopy.

2. EXPERIMENTAL SECTION

2.1. Materials. All solutions were made using ultrapure water and ACS-grade reagents. Volumetric flasks were cleaned with aqua regia and rinsed with copious amounts of ultrapure water. The reagents used for the synthesis of nanostars were tetrachloroauric(III) acid trihydrate (Acros Organics, CAS 16961-25-4), silver nitrate (Fisher Chemical, CAS 7761-88-8), and L-ascorbic acid (L-AA; Fisher Chemical, CAS 50-81-7). Stock solutions of candidate stabilizing agents were made using trisodium citrate dihydrate (Ct; Fisher Scientific, CAS 6132-04-3), disodium L-tartrate (Tt; Alfa Aesar, CAS 6106-24-7), sodium acetate (Ac; Fisher Scientific, CAS 127-09-3), sodium carbonate monohydrate (Spectrum, CAS 5968-11-6), sodium hydroxide (Fisher Scientific, CAS 1310-73-2), 1,3-propanedisulfonic acid disodium salt (PrSulf; Alfa Aesar, CAS 36589-58-9), sodium nitrate (Acros Organics, CAS 7631- 99-4), disodium sulfite (Acros Organics, CAS 7757-83-7), and disodium sulfate decahydrate (Aldrich, CAS 7727-73-3). The reference surfactant-stabilized formulation was prepared using cetyltrimethylammonium bromide, CTAB (Aldrich, CAS 57-09-0). SERS activity was probed using CV as a model analyte (Acros Organics, CAS 548-62-9, C.I. 42555, Basic Violet 3), while proof-of-concept data on the importance of the surface environment for the detection of nonideal analytes were obtained with fentanyl analogs acrylfentanyl (N-phenyl-N-[1-(2-phenylethyl)-4-piperidinyl]-2-propenamide monohydrochloride, Cayman Chemical, CAS 79279-03-1) and benzylfentanyl (N-phenyl-N-[1-(phenylmethyl)-4-piperidinyl]-propanamide, monohydrochloride, Cayman Chemical, CAS 5156-58-1).

2.2. Methods. 2.2.1. Synthesis of Nanostars. Nanostars (NS) were prepared in as-received glass vials wrapped in aluminum foil, following one of the protocols published by He et al., ¹⁷ with a post-synthetic modification. Briefly, $36~\mu L$ of 10^{-2} M HAuCl₄ and $2~\mu L$ of 10^{-2} M AgNO₃ were added to 1 mL of ultrapure water and vortexed for 10 s. Subsequently, $6~\mu L$ of 10^{-1} M L-ascorbic acid was added all at once to the reactant mixture and vortexed for 20 s. An aliquot of the candidate stabilizer, at an initial concentration of 1 M, was then added to the formed nanostars and vortexed for 5 s (Table S1 in the Supporting Information). The resulting colloidal nanostar formulations were teal in color and had a pH that varied between 4.0 and 9.5, depending on the formulation.

Unless otherwise specified, the colloidal formulations were incubated at room temperature for at least 12 h before usage.

2.2.2. Synthesis of Reference Nanospheres. Reference AuAg nanospheres (NSph) for shape versus surface chemistry effect studies were prepared in an analogous way as described for the nanostars, following one of the protocols published by He et al., 17 which makes use of 4 μL of 10^{-1} M L-ascorbic acid in place of the 6 μL required for the synthesis of the branched morphology. Disodium carbonate monohydrate, at a final concentration of 0.96 \times 10^{-3} M (Table S1 in the Supporting Information), was then added to the formed NSph and vortexed for 5 s. The resulting colloidal nanospheres were bright pink in color and had a pH of 6.5–7. The colloidal NSph were incubated at room temperature for at least 12 h before usage.

2.2.3. *Electrophoretic Light Scattering*. Electrophoretic mobility and conductivity measurements of the colloidal formulations were performed via ELS using a Malvern ZEN3600 Zetasizer and a disposable folded capillary DTS1070 Zeta cell. Standard operating procedures were created utilizing water as the dispersant and assuming the sample viscosity to be the same as the dispersant viscosity. ELS studies were performed according to two different procedures, depending on their purpose. For the initial optimization of the stabilizers' concentration, nanostar formulations were prepared in triplicate and analyzed as 800 µL aliquots. Each measurement consisted of 20 sub-runs and was subjected to a mean effective applied voltage of 148.4 V. Samples were equilibrated at 25 °C for 120 s prior to the start of the measurement (vide infra). For the estimate of the adsorption constant of the model candidate stabilizer citrate onto the bimetallic nanostars (NS/Ct system), three NS/Ct batches per each citrate concentration point were analyzed each in triplicate (N = 9)as 800 µL aliquots; the concentration of citrate in the final formulation ranged from a minimum of 1.9×10^{-4} M to a maximum of 5.2×10^{-3} M. Each measurement consisted of 25 sub-runs and was subjected to a mean effective applied voltage of 148.4 V. Samples were equilibrated for 240 s at two different temperatures: 10 and 20 °C. Temperature control was achieved by utilizing the built-in thermostatted cell holder of the instrument. The dispersant's viscosity, refractive index, and dielectric constant were set for each temperature as reported in Table S2 in the Supporting Information. The viscosity and dielectric constant were obtained by published tabulated data,35,36 while the refractive index was calculated utilizing the method published by Bashkatov and Genina.3

 ζ potential values were obtained from the measured electrophoretic mobilities (μ) as calculated using Zetasizer software ³⁸

$$\mu = 2\varepsilon_{\rm r} 3\eta \zeta f(\kappa a) \tag{5}$$

where $\varepsilon_{\rm r}$ is the dielectric permittivity of the dispersant, η is the viscosity of the dispersant, and $f(\kappa a)$ is Henry's function, which can be approximated to 1.5 for colloidal suspensions in aqueous media (Smoluchowski approximation). The use of this simple model is justified by the IUPAC's guidelines when the purpose of the electrokinetic study is the "identification of a plateau in the adsorption of an ionic species indicating optimum dosage for a dispersing agent". For the estimate of the adsorption constants, a more quantitative method as published by Ohshima was utilized to derive the ζ potential values from the measured electrophoretic mobilities. The utilized equation is as follows 1

$$\mu = \varepsilon_r \varepsilon_0 \eta \zeta f(\kappa a) \tag{6}$$

where $\varepsilon_{\rm r}$ and ε_0 are the dielectric permittivities of the dispersant and vacuum, respectively, η is the viscosity of the dispersant, and $f(\kappa a)$ is Henry's function, which in this case can be approximated to the following expression⁴¹

$$f(\kappa a) \approx \frac{2}{3} \left\{ 1 + \frac{1}{2 \left\{ 1 + \left[\frac{2.5}{\kappa a} \right] [1 + 2e(\kappa a)] \right\}^3} \right\}$$
 (7)

where a is the radius of curvature of the nanostructure ²⁴ [m] (Table S3 in the Supporting Information) and κ is the Debye–Hückel parameter [m⁻¹] (eq S1 and Table S4 in the Supporting Information). The Ohshima method is valid for all particle geometries ⁴¹ and was successfully utilized by Haes's group ²⁴ for quantitative studies on colloidal monometallic gold nanostars.

2.2.4. Extinction and UV/Vis Absorption Spectroscopy. Extinction spectra of colloidal nanoparticles were obtained with a Varian Cary 100 Bio UV/Vis spectrophotometer fitted with a tungsten halogen lamp with a quartz window as a visible light source, a deuterium arc lamp as an ultraviolet light source, a Czerny-Turner 0.28 M monochromator, and a highperformance R928 photomultiplier detector. All measurements were performed in a single-beam arrangement in the 400-900 nm range with automatic baseline correction. The same instrument and instrumental specifications were utilized to collect UV/Vis absorption spectra of CV, in the 200-900 nm range. Decay curves for each nanostar formulation were obtained by acquiring a series of extinction spectra, each at 10 min intervals, for a total of 2 h, immediately after synthesis. The mean and standard deviation of the intensity at the λ_{LSPR} for each time point were first converted to the percent decrease from initial values at time zero and then plotted against time. All measurements were performed in triplicate.

2.2.5. X-ray Photoelectron Spectroscopy. Surface analysis of NS/Ct was performed at the Research Service Centers, Herbert Wertheim College of Engineering, University of Florida, Gainesville. An ultrahigh-vacuum Phi VersaProbe III scanning X-ray photoelectron spectrometer was used for both survey and high-resolution spectral acquisitions. The survey scan was collected using a monochromatic Al K α source with 93.90 eV passing energy; high-resolution spectra were acquired using a passing energy of 11.75 eV (Au, 4f) and 23.50 eV (Ag, 3d; C, 1s). A 5 mm² microscopy-grade glass substrate was sonicated once in acetone for 20 min and then twice in methanol for 20 min each time. The substrate was left to dry inside a clean, closed container. A 1 μ L aliquot of concentrated (vide infra) citrate-capped colloidal nanostars was then deposited onto the prepared glass substrate and left to dry at room temperature inside a clean, closed container. The concentrated formulation was obtained by centrifugation of a total volume of 1045 μ L NS/Ct for 1 min at 5000 rpm and subsequent removal of 990 µL of supernatant. Peak deconvolution and integration of components were performed using CasaXPS software (v2.3.19PR1.0 demo, Casa Software Ltd, Teignmouth, UK).

2.2.6. Transmission Electron Spectroscopy. Morphological studies were conducted via transmission electron microscopy (TEM) at the Advanced Materials Engineering Research Institute (AMERI) at Florida International University. TEM micrographs were obtained using a Philips CM200 trans-

mission electron microscope with a point and line resolution of 0.1 and 0.14 nm, respectively. A total of 8 mL of each nanostar formulation was deposited on a copper grid and dried at room temperature for approximately 30 min before analysis. Micrograph processing was performed using ImageJ v1.53a. 42

2.2.7. Normal Raman and Surface-Enhanced Raman Spectroscopy. Normal Raman and SERS measurements were performed using a PerkinElmer 400 F Raman benchtop spectrometer fitted with a 785 nm laser excitation source (350 mW power at the source, 100 mW power at the sample 0.05 nm fwhm) and a high-sensitivity air-cooled (-50 °C) CCD detector. The resolution was 4 cm⁻¹ FWHM, and the exposure time was set to 10 s with four accumulations for all spectral acquisitions. All samples were analyzed in 250 μL solution aliquots and deposited in a 96-well quartz microplate (Hellma Analytics). SERS samples of the model analyte CV were prepared by mixing 247.5 µL of colloidal nanostar formulation and 2.5 µL of CV aqueous solution at a final concentration of 10⁻⁷ M. SERS samples of fentanyl analogs were analyzed with prior aggregation instead by mixing 245 μ L of colloidal nanostar formulation with 2.5 µL of 1.67 M MgCl₂, followed by addition of 2.5 μ L of fentanyl analog methanolic solution at a final concentration of 10 ng/mL. All SERS samples were incubated for 20 min. All SERS and normal Raman spectra were baseline-corrected, and the intensities were normalized to the intensity of the band at 3200 cm⁻¹, assigned to $\nu(OH)$ of

2.2.8. Statistical Analysis. Exploratory data analysis via a box-and-whiskers plot, analysis of equal variances, and test for normality were performed with Minitab statistical software (v17.1.0, Minitab Inc., State College, PA). Analysis of Variance (ANOVA) *F*-test, Tukey–Kramer's test, and Student's *t*-test were performed with JMP statistical software (v15, SAS Institute, Cary, NC).

2.2.9. FTIR Spectroscopy. Infrared spectroscopy measurements were performed in the attenuated total reflection (ATR) mode using an Agilent Technologies Cary 670 FTIR spectrometer fitted with a PIKE MIRacle single-reflection ATR accessory with a diamond internal reflection element (IRE) and interfaced with Agilent Resolutions Pro software. Samples were obtained by pooling 35 mL of each colloidal nanostar formulation; an aliquot of 3 mL was kept for UV/Vis absorption spectroscopy, while the remaining volume was centrifuged at 5000 rpm for 15 min. Subsequently, 30 mL of supernatant was replaced with an equivalent amount of ultrapure water to ensure removal of unadsorbed capping species and then centrifuged again at 5000 rpm for 15 min. A total of 29 mL of supernatant was then removed, and the remaining volume was dried under vacuum centrifugation at room temperature for approximately 7 h. The dried residues were then aliquoted in three sub-samples and placed on the IRE for analysis. Additionally, 1 M solutions of candidate stabilizing agents were analyzed by placing 2 μ L of solution on the IRE. The acquisition method was the same for both solid and liquid samples and consisted of 128 preliminary background scans and 128 sample scans, each at a resolution of 2 cm^{-1} .

3. RESULTS AND DISCUSSION

3.1. Part 1: Selection of Candidate Alternative Stabilizing Agents and Optimization of Colloidal Formulations. In its simplest meaning, DLVO theory states that in order to increase the stability of a colloidal suspension,

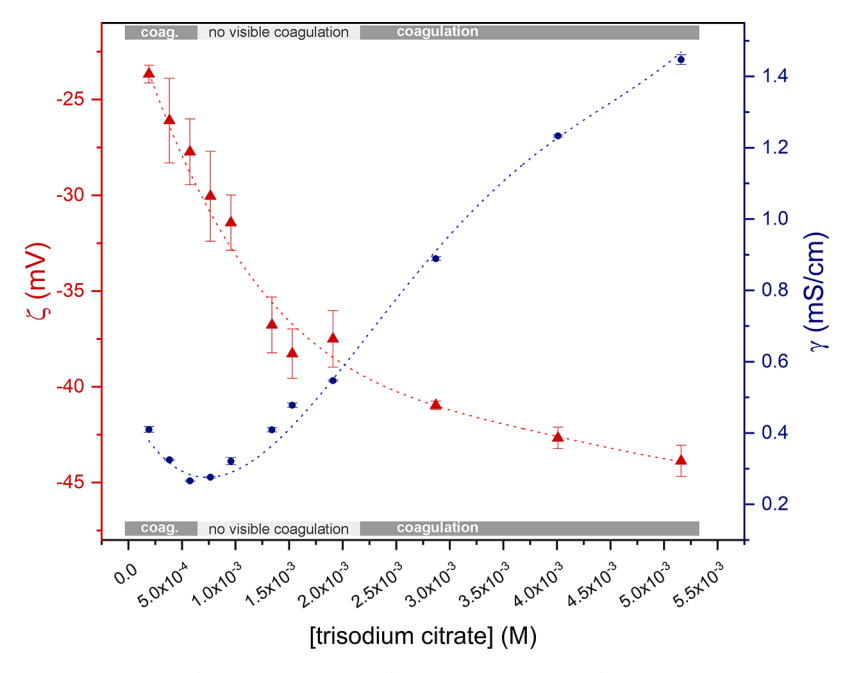


Figure 1. ζ potential (red triangles, left *y*-axis) and conductivity (blue dots, right *y*-axis) behavior of AuAg colloidal nanostars titrated with trisodium citrate. The error bars report the standard error for each measured point. The data trend is highlighted by polynomial fits (dotted lines). The gray bars indicate the visual observations of the coagulation status of the samples at the time of analysis. For information on the relationship between the ζ potential and conductivity, the reader is referred to publications such as O'Brien⁵⁰ and Ohshima.

the Coulombic repulsive forces at the particle–solution interface must be maximized. $^{29,31-34}$ To accomplish this, two variables must be determined: first, the charge sign of the stabilizing species and, second, the identity of this species. As reported in the Introduction, the as-synthesized nanostars are unstable, as demonstrated by their rapid coagulation (Figure S1) and their ζ potential of -19.9 ± 3.2 mV. As a rule of thumb, systems having absolute values of ζ potential between 0 and |25| mV are considered unstable. 43 The ζ potential sign of the as-synthesized nanostars was negative, indicating that the capping species population was predominantly negatively charged. Thus, anionic species should be added to the formulation to maximize the Coulombic repulsions.

Our hypothesis was that nanostar capping would occur as a result of chemisorption (i.e., covalent or coordinating covalent adsorption). This hypothesis implies that the nanostar's surface is predominantly in its zero oxidation state and is supported by the experimental findings of Al-Johani et al.²¹ for monometallic gold nanospheres. Trisodium citrate (Ct) was selected as a prototypical, negatively charged, alternative capping agent because of its well-known stabilizing properties in traditional colloidal sol formulations. Moreover, it has much smaller dimensions compared to CTAB, the original stabilizer chosen by He et al., 17 it does not form micelles in solution, and it has a pH-tunable charge that can be exploited to further optimize the interactions between the nanostructure and the analyte. Being a highly studied compound, 21,22,44 trisodium citrate would also provide some basis for comparison with literature data. The other candidate stabilizing agents were selected by reducing the carbon chain of the prototype trisodium citrate. Assuming no displacement, the thickness of the barrier separating the analyte from the surface should be as low as possible, in order for the system to yield the strongest SERS enhancement. Disodium L-tartrate (Tt) and sodium acetate (Ac) were selected for this purpose. Since these candidate stabilizing agents all have a common characteristic (i.e., the

presence of one or more carboxylate functional groups), it may be difficult to discern whether stabilization occurs via electrostatically driven ion pairing with the surface or via a molecule-specific adsorption process (covalent adsorption on a zero-valent nanoparticle surface). For this reason, 1,3-propane-disulfonic acid disodium salt (PrSulf) was added to the list of candidate stabilizers, together with an array of inorganic polyatomic ions, namely nitrate, sulfite, sulfate, and carbonate. For all selected species, the identity of the counterion was kept constant as Na^+ .

3.1.1. Optimization of the Model Surfactant-free Formulation NS/Ct. The optimum concentration for citrate stabilization of the colloidal sol was determined via ζ potential and conductivity (γ) titrations of the as-synthesized bimetallic nanostars with increasing concentration of the anion (Figure 1). The ζ titration determined the concentration of citrate at which the maximum absolute value of ζ potential was observed, corresponding to the point of maximum occurrence of Coulombic repulsions, hence maximum colloidal stability. As expected, the ζ titration curve showed increasingly negative ζ potential values with increasing concentration of citrate (Figure 1). By definition, this indicates that the citrate ions are present in a region between the surface of the nanostructure and its slipping plane. While no deduction on whether citrate adsorbs electrostatically or covalently can be made, it can be reasonably assumed that the change in the ζ potential is caused by a change in surface charge density. For this reason, the change in the ζ potential reflects surface adsorption, regardless of the specific mechanism. Indeed, for colloidal sols in which the surface charge density is proportional to the ion concentration, which is the case for these titrations, it has been demonstrated that the following equation is

$$\psi_0 = \zeta \left(1 + \frac{1}{\kappa a} \right) e \tag{8}$$

Table 1. Average ζ Potential and Conductivity Values for a Series of AuAg Nanostars Formulations, at Fixed Concentration of the Candidate Stabilizer (0.96 × 10⁻³ M) and Fixed Molar Ionic Strength of the Formulation (3.4 × 10⁻³ M)^a

				· ·		
formulation	candidate stabilizer	characteristics	ζ potential \pm std error (mV)	ζ potential compared to the baseline value	conductivity \pm std error (mS/cm)	conductivity compared to the baseline value
NS	none		-17.2 ± 0.2	baseline value	0.590 ± 0.002	baseline value
NS/Ct	citrate	optimized conc	-35 ± 1	1	0.329 ± 0.007	1
$NS/Tt_{(c)}$	L-tartrate	[anion] = const	-30.3 ± 0.6	↑	0.334 ± 0.001	↓
$NS/Tt_{(I)}$	L-tartrate	$I_{ m formulation} = { m const}$	-32.0 ± 0.9	↑	0.3800 ± 0.0007	↓
NS/Ac _(c)	acetate	[anion] = const	-22 ± 1	1	0.287 ± 0.006	1
NS/Ac _(I)	acetate	$I_{ m formulation} = { m const}$	-28.6 ± 0.9	1	0.4100 ± 0.0003	Ţ
NS/CO ₃ ²⁻ (c)	carbonate	[anion] = const	-34 ± 1	1	0.232 ± 0.004	1
NS/CO ₃ ²⁻ (I)	carbonate	$I_{ m formulation} = { m const}$	-33.3 ± 0.3	1	0.640 ± 0.005	↑
NS/PrSulf _(c)	1,3-propanedisulfonic acid disodium salt	[anion] = const	-23.3 ± 0.4	1	0.690 ± 0.007	↑
NS/PrSulf _(I)	1,3-propanedisulfonic acid disodium salt	$I_{ m formulation} = { m const}$	-24.5 ± 0.6	1	0.8000 ± 0.0006	↑
NS/SO ₃ ²⁻ (c)	sulfite	[anion] = const	-24.8 ± 0.4	1	0.359 ± 0.003	1
NS/SO ₃ ²⁻ (I)	sulfite	$I_{ m formulation} = { m const}$	-21.8 ± 0.9	1	0.570 ± 0.003	↓
NS/SO ₄ ²⁻ (c)	sulfate	[anion] = const	-25.3 ± 0.2	1	0.714 ± 0.006	↑
NS/SO ₄ ²⁻ (I)	sulfate	$I_{ m formulation} = { m const}$	-8 ± 5	1	0.81 ± 0.04	↑
NS/NO ₃ ⁻ (c)	nitrate	[anion] = const	-25.2 ± 0.2	1	0.718 ± 0.006	1
NS/NO ₃ ⁻ (I)	nitrate	$I_{ m formulation} = { m const}$	-23.1 ± 0.4	1	0.9400 ± 0.0006	1
NS/OH ⁻ (c)	hydroxyl ion	[anion] = const	-22.7 ± 0.5	1	0.276 ± 0.005	↓
NS/OH ⁻ (I)	hydroxyl ion	$I_{ m formulation} = { m const}$	-36.5 ± 0.8	1	0.390 ± 0.001	↓

[&]quot;All counterions are Na $^+$; average values are followed by their standard error. Underlined ζ potential values are those whose average exceeds the nominal absolute value for colloidal stability (|25| mV). A more visual representation of these data can be found in Figure S5 in the Supporting Information.

where ψ_0 is the surface potential, κ^{-1} is the Debye length, a is the radius of curvature of the smallest nanoparticle feature, ²⁴ and e is Euler's number.

Another indication that surface adsorption is occurring is given by the trend described by the ζ titration curve, which resembles an upside-down Langmuir or class L^{48,49} adsorption isotherm. The measured variable linearly increases in absolute value until a threshold is reached, which can be interpreted as an indication of monolayer saturation of the available adsorption sites (Figure S2a). This could be followed by either no further adsorption or the formation of ad-layers (Figure S2b-d).

It is also interesting to observe the simultaneous behavior of conductivity (γ) and its relationship with the shape of the ζ titration curve. The conductivity is observed to initially decrease, as a result of the adsorption of citrate; this likely leads to the formation of a hybridized material, the capped nanoparticle, with different specific conductivities from the unmodified, sparingly capped nanoparticle. Alternatively or concomitantly, the conductivity decrease could be linked to the participation of solution counterions in the formation of the electric double layer, thus decreasing the population of free ions in solution.

After this initial conductivity decrease, an inversion point is observed at 0.77×10^{-3} M citrate, after which the conductivity increases linearly with citrate concentration. This can be explained using the ζ titration curve and the Langmuir model as references. There is a concentration, 1.3×10^{-3} M, at which the system starts to approach its supposed maximum monolayer adsorption capacity. At saturation, the available adsorption sites are all occupied, and the addition of excess adsorbate molecules (i.e., citrate) increases the ionic population of the solution environment, rather than that of the surface. This causes conductivity to rise. However, it must be noted that it cannot be determined whether the adsorption behaves strictly in a Langmuir fashion or if formation of adlayers occurs instead. More on this topic is presented in Section 3.3.1 of this paper.

Figure 1 can also be utilized to explain the coagulation behavior of the various NS/Ct formulations. It was observed that coagulation happens not only at the lowest concentrations of citrate but also at the highest, despite the ζ potential being high (>|25| mV) in magnitude (Table S3). The Debye length is inversely proportional to the ionic strength of the solution constituting the dispersing phase of the colloidal sol and dictates the thickness of the nanoparticle's electrical interfacial layer. Therefore, at higher ionic strengths, the Debye length

gets compressed, ultimately decreasing the distance at which flocculation and eventually coagulation occur (Figure S3). The concomitant high-magnitude ζ potential of these higher ionic strength formulations can be explained by recalling that coagulation is a dynamic process, and the extent to which it occurs varies with time; at time 12 h, two populations are present in the solution—a coagulating population and a still-dispersed population.

According to Figure 1 and the visual observations reported in Table S3, there was more than one colloidal formulation that achieved short-term stability. However, since coagulation can also be induced by the addition of analyte solution (i.e., at the SERS sample preparation level), 52 it is wise to choose as the optimum formulation a citrate concentration that is not too close to the observed coagulation extremes (gray bars in Figure 1) and that has the lowest ionic strength and conductivity as possible. This helps to avoid an overly rapid coagulation upon the addition of sample solutions when utilizing these colloidal nanoparticles as SERS substrates. As a result of these observations, the optimal concentration of citrate was 0.96 × 10⁻³ M. This concentration causes an increase in molar ionic strength of 3.4×10^{-3} M compared to the unmodified nanostars', bringing the total molar ionic strength of the optimized NS/Ct formulation to 3.8×10^{-3} M. TEM micrographs of this formulation are reported in Figure S4.

The colloidal formulation containing 0.96×10^{-3} M citrate showed no visual signs of coagulation for over four months. On the other hand, the formation of flocs was observed after a period of approximately 48 h. Flocs are reversible aggregates that are a result of a secondary minimum in the free energy DLVO curve of the order of few $k_{\rm B}T$, where $k_{\rm B}$ is Boltzmann's constant and T is the absolute temperature, such that regular Brownian motion provides the sufficient energy for collision and reversible formation of aggregates. The energy provided by manual shaking for approximately 2 s was sufficient to fully redisperse the colloidal sol.

3.1.2. Screening of Other Candidate Stabilizers by ELS. ζ potential and conductivity measurements were also performed for the remainder of the candidate stabilizers, with the aim of exploring the effect of the negatively charged functional group on the capping process. These species were screened at $0.96 \times$ 10⁻³ M (the optimal concentration for citrate) and at a second concentration which was adjusted to the same molar ionic strength $(3.4 \times 10^{-3} \text{ M})$ as the formulation containing citrate. As shown in Table 1 and Figure S5, both datasets, at constant concentration and at constant molar ionic strength, display a similar trend, although the formulations at constant ionic strength showed a more pronounced division into two distinct groups: effective candidate stabilizers and ineffective candidate stabilizers. Compounds containing at least one carboxylate functional group or even a carboxylate-like structure such as disodium carbonate increased the ζ potential past the threshold for nominal colloidal stability ($|\zeta| \ge |25| \text{ mV}$). This ζ potential increase was accompanied by a simultaneous decrease in conductivity compared to the baseline levels of the as-synthesized nanostars (NS, shaded row in Table 1), similar to that observed for citrate in the concentration range preceding monolayer saturation (Figure 1, Section 3.1.1). These trends are not observed for the remainder of the surveyed anionic species, which either maintained the ζ potential around that of the as-synthesized nanostars or decreased it, while a parallel increase in the conductivity was recorded. For these formulations, a rapid onset of coagulation

was observed (Table S5). None of the anionic species in this second group had any carboxylate function in their structure or did they possess a carboxylate-resembling group, such as carbonate. These results suggest a connection between the molecular structure of a candidate stabilizer and its ability to effectively cap the bimetallic nanostructure and provide stability. This supports our hypothesis that capping and thus stabilization are a result of chemisorption (i.e., covalent or coordinating covalent adsorption) rather than a consequence of the retention of electrostatically adsorbed anions. This is in line with our XPS observations (Section SD in the Supporting Information), which indicated that the metals comprising the nanostars, gold and silver, are alloyed and in their elemental oxidation state. These results are consistent with those reported by Al-Johani et al.²¹ for monometallic gold nanospheres, supporting our hypothesis that the surface of the bimetallic nanoparticle is in its zero oxidation state. A more extensive discussion of these results is reported in the Supporting Information (Section SD, Figures S6–S8).

Carbonate was the candidate stabilizer which brought the ζ potential to the most negative values, with maximum stability across the surveyed formulations, both at constant molar ionic strength and at constant concentration. This was an unexpected finding in that inorganic salts are typically used to induce controlled aggregation and coagulation and thus to cause instability. This unexpected stabilizing effect could be caused by either a structural similarity with the carboxylate functional group, which appears to provide efficient capping of the bimetallic nanostructures, or by the fact that carbonate is an alkalinizing agent. There is evidence that hydroxyl ions, such as those normally produced in an aqueous solution of disodium carbonate, are able to adsorb to nanoscale gold. 54,55 However, the presented results are not sufficient to conclude which of the two hypotheses (chemical affinity of carbonate or alkalinity) best describes the ensuing stability of AuAg nanostars by post-synthetic addition of disodium carbonate or in which proportion the two factors are concomitantly occurring.

In light of what was observed for the two NS/CO₃²⁻ formulations and of what was mentioned about hydroxyl ion adsorption on gold surfaces, 54,55 additional experimental data at constant concentration and constant molar ionic strength were obtained by the post-synthetic addition of NaOH (last two rows in Table 1). Stability was observed for the constantmolar ionic strength preparation only; the ζ potential of the constant-concentration formulation was -22.7 ± 0.5 mV, a value that falls below the standard threshold for colloidal stability. 43 This formulation showed visual signs of aggregation after approximately 2 h (Table S5). On the other hand, the constant molar ionic strength formulation, NS/OH $_{(I)}^-$, had a ζ potential of -36.5 ± 0.8 mV and did not exhibit visual signs of coagulation. Regarding conductivity, the behavior of NS/OH⁻ followed the trend exhibited by the carboxylate-based and carbonate-based formulations, that is, conductivity decreased compared to the unmodified nanostars. This was observed for both constant concentration and constant molar ionic strength. The behavior displayed by NS/OH⁻ was similar to that of NS/ Ac. Given the demonstrated stabilizing effect of hydroxyl ions, it can be hypothesized that the mechanism by which disodium carbonate attains colloidal stability was likely caused by a combined action of both carbonate and hydroxyl ions.

3.1.3. Screening of Effective Candidate Stabilizers by Extinction Spectroscopy. Decay studies based on extinction

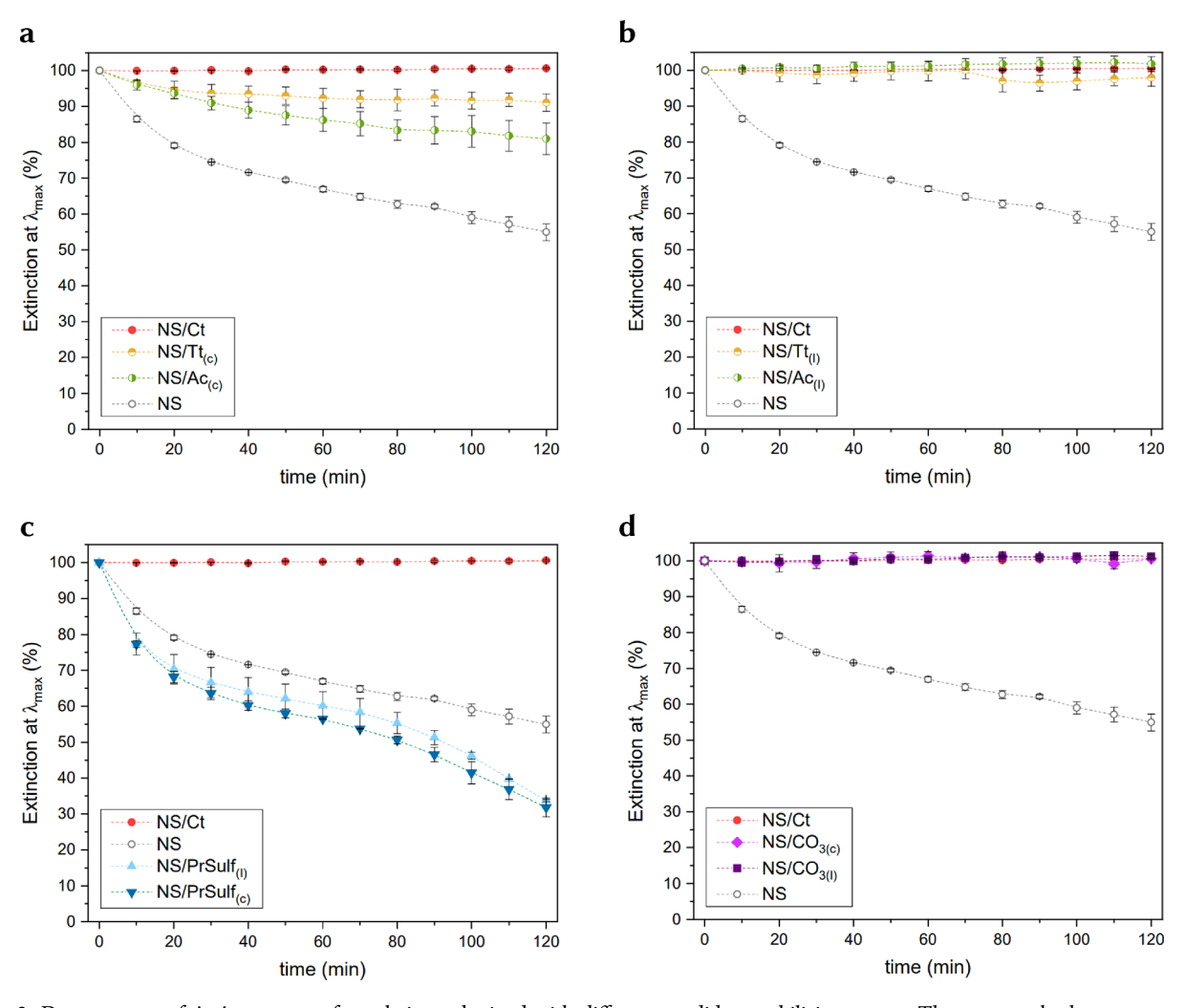


Figure 2. Decay curves of AuAg nanostar formulations obtained with different candidate stabilizing agents. The top panels show a comparison among sodium carboxylates: trisodium citrate (NS/Ct, red), disodium tartrate (NS/Tt, yellow), and sodium acetate (NS/Ac, green), (a) at a constant concentration of 0.96×10^{-3} M and (b) at a constant molar ionic strength of 3.4×10^{-3} M. (c) Comparison between the effectively stabilized formulation NS/PrSulf (1,3-propanedisulfonic acid disodium salt, negative control). NS/PrSulf at both constant concentration (light blue triangles) and at constant molar ionic strength (bottom-up indigo triangles) are shown. (d) Comparison between stabilized formulations NS/Ct and NS/CO $_3^{2-}$; both formulations at constant concentration (light-purple diamonds) and constant molar ionic strength (purple squares) are shown. All empty gray circle profiles refer to the as-synthesized nanostars with no candidate stabilizer added. Dashed B-spline connectors are used to highlight data trends; error bars represent the standard deviation. Information on the pH of each formulation can be found in Table S1 in the Supporting Information. A selection of the extinction spectra utilized for this figure (NS/Ct and NS/PrSulf) has been reported in Figure S13 in the Supporting Information.

spectroscopy were performed on the nanostar formulations prepared with the effective candidate stabilizers (Ct, Tt, Ac, and CO₃²⁻), with the twofold aim of (1) spotting any early ensuing aggregation before it was visible to the naked eye and (2) discerning which of the two formulations (constant concentration or constant molar ionic strength) had better stability. It was hypothesized that the constant-molar ionic strength formulations would display superior stability, as ionic strength, rather than nominal concentration, plays an important role in determining the Debye length and, ultimately, the interparticle distances at which aggregation occurs. The decay curves of the NS formulations stabilized with carboxylates at a fixed concentration $(0.96 \times 10^{-3} \text{ M})$ Figure 2a) exhibited increasing stability with increasing nominal charge; on the other hand, at a fixed molar ionic strength $(3.4 \times 10^{-3} \text{ M}, \text{ Figure 2b})$, all formulations showed analogous stability, with statistically constant extinction over the investigated 2 h period. As expected, this indicates that the

total, effective charge density on the surface is the key factor for stability, rather than the nominal charge per molecule. NS/ PrSulf was chosen as the model for an unstable formulation and thus as a negative control (Figure 2c). As expected from the ζ potential and conductivity survey presented in the previous section, NS/PrSulf showed the opposite behavior of the carboxylate-stabilized formulations; the stability of both the constant concentration and constant molar ionic strength formulations exhibited a steeper decay than the unmodified NS, suggesting that PrSulf does not improve the stability of the colloidal nanostars and instead accelerates their coagulation. Finally, as shown in Figure 2d, CO_3^{2-} provided stability to the colloidal nanostars at both constant concentration and constant molar ionic strength. Stability was also maintained past the 2 h window selected for the decay study with no visual signs of aggregation for up to four months. This mirrors the behavior of NS/Ct, as described earlier. Also, in this case, flocs were observed after 48 h of incubation, and the colloidal sol

was completely redispersed after approximately 2 s of manual shaking. TEM micrographs of all optimized formulations can be found in the Supporting Information (Figures S4, S9–S12).

3.2. Part 2: SERS Performance Studies. The SERS performance of the developed colloidal nanostar formulations was evaluated utilizing CV as the model analyte (Figure S14). This dye was chosen because it has been extensively characterized by both FT-Raman ($\lambda_{\rm exc}$ 1064 nm) and SERS ($\lambda_{\rm exc}$ 633 nm, citrate-reduced Ag nanospheres), and the assignment of its vibrational modes has been made via Density Functional Theory (DFT) calculations.⁵⁶ Moreover, it is offresonance with the excitation source (Figure S15), thus ensuring that the observed enhancement arises from SERS only and not from additional laser-dye resonance phenomena (i.e., Resonance Raman, RR, or Surface-Enhanced Resonance Raman, SERRS). The normal Raman spectrum of CV in aqueous solution at a concentration of 10⁻³ M and neutral pH is reported in Figure S16a, while Figure S16b shows the SERS spectrum of the same dye at a concentration of 10^{-7} M. The SERS spectrum was obtained using the NS/Ct formulation with no aggregating agent added. The assignment of the vibrational modes is reported in Table S6 and was performed by comparison with previously published DFT calculation data. 56 It must be noted that the differences in the band position between the normal Raman and SERS spectra of CV are negligible and no changes in the bands' relative intensity are observed. This suggests that the dye is physisorbing onto the nanostars, rather than chemisorbing. The latter phenomenon would in fact produce changes in the spectral profile, especially in terms of the band position, because the analyte should change its electronic environment upon complexation with the substrate. Physisorption of CV is also reported to occur on traditional citrate-reduced monometallic silver nanospheres.50

The band at 1170 cm⁻¹, assigned to the ensemble of $\nu_{\rm s}({\rm CC}_{\rm center}{\rm C})$, $\delta({\rm CCC})_{\rm breathing}$, and $\rho({\rm CH}_3)$ vibrational modes, 56 was selected as the marker band for this performance study. This band was reported to originate from totally symmetric (a₁) modes;⁵⁶ therefore, its intensity is directly and exclusively related to the effect of the electromagnetic enhancement.⁵⁷ This is particularly important for the evaluation of the analytical enhancement factor (AEF). Because the intensity of a totally symmetric band is expected to be governed by the electromagnetic enhancement only and because the electromagnetic enhancement directly depends on the analyte-substrate distance, the effect of the varying capping layer thicknesses among the different NS formulations on the magnitude of the AEF can be evaluated. The incubation time of the analyte and NS mixture was determined by studying the evolution of the intensity profile over time, as reported in the Supporting Information (Section SH).

Before studying the SERS performance of the NS formulations, it was important to determine the reproducibility of their optical properties. This ensured that any deviation in performance among different NS formulations was not linked to synthesis-related plasmon band variability. These studies are discussed in length in the Supporting Information (Section SJ), resulting in best practice recommendations for the analytical application of these nanomaterials. For best reproducibility of the SERS response, pooled NS samples should be utilized as enhancing substrates, as opposed to individual ≈ 1 mL batches; if individual batches are to be utilized, measurement of the $\lambda_{\rm LSPR}$ should be strictly performed prior to the SERS

measurement(s), and an inter-batch $\lambda_{\rm LSPR}$ tolerance of ± 15 nm should be adopted. More information on the rationale behind this interval is reported in Section SJ in the Supporting Information. A morphological yield study was also performed by analyzing model formulation NS/Ct (Section SK in the Supporting Information); as demonstrated by the TEM micrographs in Figures S4 and S9–S12, the post-synthetic addition of the utilized stabilizers does not alter the nanostar morphology.

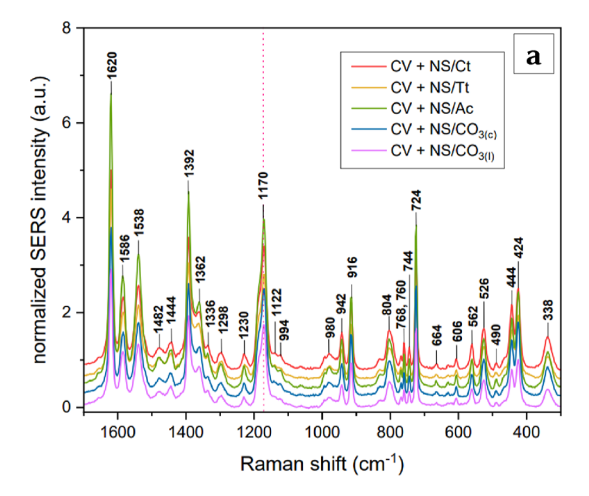
After these preliminary characterization studies, the two performance parameters that were investigated were the AEF and the long-term stability, the latter involving the determination of the shelf life of the formulations. The most stable formulation was then utilized with nonideal probes acrylfentanyl and benzylfentanyl to provide proof-of-concept data that demonstrate that the effect of the surface environment may be more conducive than the effect of morphology in achieving high-intensity SERS signals (Section SL in the Supporting Information).

3.2.1. AEF as a Function of Capping Species. An overview of the SERS spectra of CV obtained using each formulation of nanostars, NS/Ct, NS/Tt, NS/Ac, NS/CO₃²⁻(c), and NS/ CO₃²⁻(1), is given in Figure 3a. When comparing these spectra with the reference Raman spectrum of CV (Figure S16a), it can be observed that no foreign bands were present for any of the formulations, indicating that the capping species do not interfere with the analyte's signal. This lack of interference could be the result of displacement of the capping species by the analyte, a small SERS cross-section of the capping species, or a combination of the two. The band intensity of the spectra obtained with these modified NS formulations is 7-13 times higher than that obtained by utilizing the original 17 NS/CTAB formulation, and the band resolution is also improved, as shown in Figure 3b. A way to quantify these differences is by calculating the AEF, as defined by Le Ru et al.⁵⁸

$$AEF = \frac{\frac{I_{SERS}}{c_{SERS}}}{\frac{I_{NR}}{c_{NR}}}$$
(9)

where $I_{\rm SERS}$ is the intensity of the SERS signal at a given reference band, $c_{\rm SERS}$ is the concentration of CV in the SERS experiment, $I_{\rm NR}$ is the intensity of the normal Raman signal at the same reference band, and $c_{\rm NR}$ is the concentration of CV in the Raman experiment. This definition was chosen because it provides a reproducible method for presenting the signal magnification produced by colloidal sols.⁵⁸

To calculate the AEF, the SERS profile of CV adsorbed on each of the abovementioned NS formulations and on NS/ CTAB was measured 24 h after synthesis, under a fixed set of experimental conditions (see the Methods section). Table 2 shows the mean intensities at 1170 cm⁻¹ for CV, for both Raman and SERS spectra obtained with the various NS formulations, together with the associated AEF values. The AEF values for CV using the newly developed NS formulations are all within the same order of magnitude, ranging from a minimum of 0.8×10^5 to a maximum of 1.6×10^5 , while the CV + NS/CTAB system (N = 3) had an AEF 3 orders of magnitude smaller (4.1×10^2) . As reported in Figure 4a and Tables S25-S27, the ANOVA F-test and Tukey-Kramer's test on the AEF values showed that the CV + NS/CTAB system is significantly different from all other systems ($F_{5,27}$ critical < Fvalue 45.0495, p value < 0.0001 > α 0.05; Tukey Kramer's p-



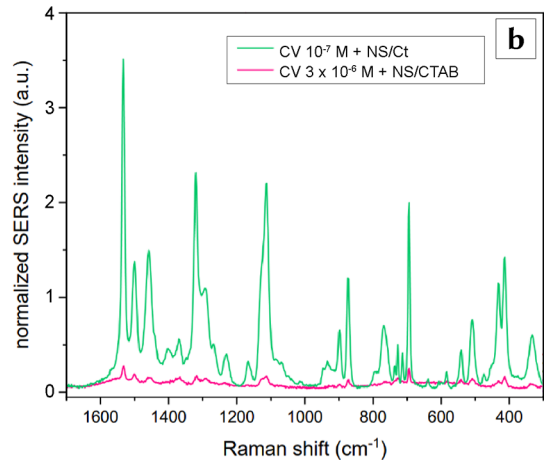


Figure 3. (a) SERS spectra of CV at a concentration of 10^{-7} M, obtained using each of the developed alternatively stabilized NS formulations as the enhancing substrate. In order from top to bottom: NS/Ct (red), NS/Tt (yellow), NS/Ac (green), NS/CO₃²⁻_(c) (blue), and NS/CO₃²⁻_(l) (purple). (b) Comparison between the CV spectrum obtained with NS/Ct as the enhancing substrate (green) and that of CV obtained with the original PNS/CTAB formulation (pink, bottom). All spectra were baseline-corrected, and their intensities were normalized to the intensity of the band at 3200 cm⁻¹, assigned to ν (OH) of water. Spectra in (a) are stacked for ease of comparison.

Table 2. Normalized SERS and Raman Intensities at CV's Marker Band 1170 cm⁻¹ and AEF Values for Each of the CV-NS Systems

system	mean AEF (×10 ⁵)	AEF std error $(\times 10^5)$
CV + NS/Ct	1.6	0.9
CV + NS/Tt	1.4	0.7
CV + NS/Ac	1.5	0.4
$CV + NS/CO_3^{2-}$ _(c)	1	1
$CV + NS/CO_3^{2-}(I)$	0.8	0.4
CV + NS/CTAB	0.0041	0.0001

value < 0.0001 for all pairs). The CV + NS/CO₃²⁻₍₁₎ system was also found to be significantly different from the other systems (Table S28). This finding was unexpected since the NS/CO₃²⁻₍₁₎ formulation does not have any bulky capping agent and has the most negative ζ potential, which should increase the likelihood of ionic pairing between the capped surface of the nanoparticle and the positively charged CV. The

only factor that could be negatively impacting the AEF is pH. The NS/CO₃²⁻(I) formulation is the only one of the set that has an alkaline pH, 9.5, and triarylmethane dyes such as CV are known to undergo basic hydrolysis (Figure S33). The hydrolyzed bond participates in the normal modes associated with the 1170 cm⁻¹ band utilized as a marker for CV, ν_s (CC_{center}C), δ (CCC) breathing, and ρ (CH₃), causing a decrease in its intensity.

In order to elucidate whether pH could be the possible cause of the significantly different AEF of the NS/CO₃²⁻(I) when compared to the other new formulations, a second set of analogous SERS measurements was performed utilizing the NS/OH-(I) formulation. This formulation was previously utilized as a control in the initial stabilization studies, and because it has a pH of approximately 9.5, like $NS/CO_3^{2-}(I)$, it could be utilized as an additional point of comparison for measurements of CV under alkaline conditions. An ANOVA Ftest followed by Tukey-Kramer's test allowed two groups to be identified (Figure 4b and Tables S29 to S32): the first one containing the NS formulations that have neutral or acidic pH and the second containing the NS formulations having alkaline pH. This result supports the hypothesis that the lower AEF observed for the CV + NS/CO_3^{2-} _(I) system can be attributed to the basic hydrolysis of CV, which causes the band at 1170 cm⁻¹ to decrease, resulting in a lower AEF.

Despite the difference between NS/CO₃²⁻_(I) and the rest of the new formulations, this study validates the hypothesis that the alternatively stabilized formulations have superior SERS activity than the original¹⁷ surfactant-capped formulation. This can be attributed to the decreased thickness of the alternative capping agent when compared to the CTAB bilayer and to their possible displacement by CV.

3.2.2. Shelf Life of the New NS Formulations. Together with substrate reproducibility, shelf life is another critical element for establishing recommendations for the use of colloidal sols in analytical practice. However, no guideline for shelf life determination of colloidal nanoparticles has been issued yet. As a result, a new methodology was established, borrowing concepts from pharmaceutical industry protocols and based on the combined use of one-tailed and double-tailed Student's *t*-test to study the intensity of the CV marker band over time, as illustrated in detail in Section SN in the Supporting Information.

The results are shown in Table S36, and the shelf life estimates are summarized in Table 3. As expected from visual observations, the formulation with the shortest shelf life was NS/Tt, whose time points were all significantly different from the reference dataset at t_0 , with Prob > |t| of 0.0407 and 0.0005 for the 2-week and 1-month time points, respectively. The NS/ Ct and NS/CO₃²⁻_(c) formulations had the longest shelf life; the NS/Ct formulation had no significant changes at the 2week time point (Prob > |t| 0.2472) but did have significant differences at the two successive time points of 1 and 4 months, with Prob > Itl of <0.0001 and 0.0266, respectively. While no signs of coagulation were observed, some level of aggregation had in fact occurred, as the Prob > t was <0.0001for the 1 month mark and 0.0133 for the 4 months mark. As for the $NS/CO_3^{\ 2-}{}_{(c)}$ formulation, the SERS intensities at the second week were flagged as significantly different from the $t_{\rm 0}$ reference, with a Prob > |t| of <0.0001. Since the right-tailed test yielded a Prob > t of 1.0000, which is not significant, and since no accompanying discoloration of the sol was observed (Table S34), this point was treated as an anomaly.

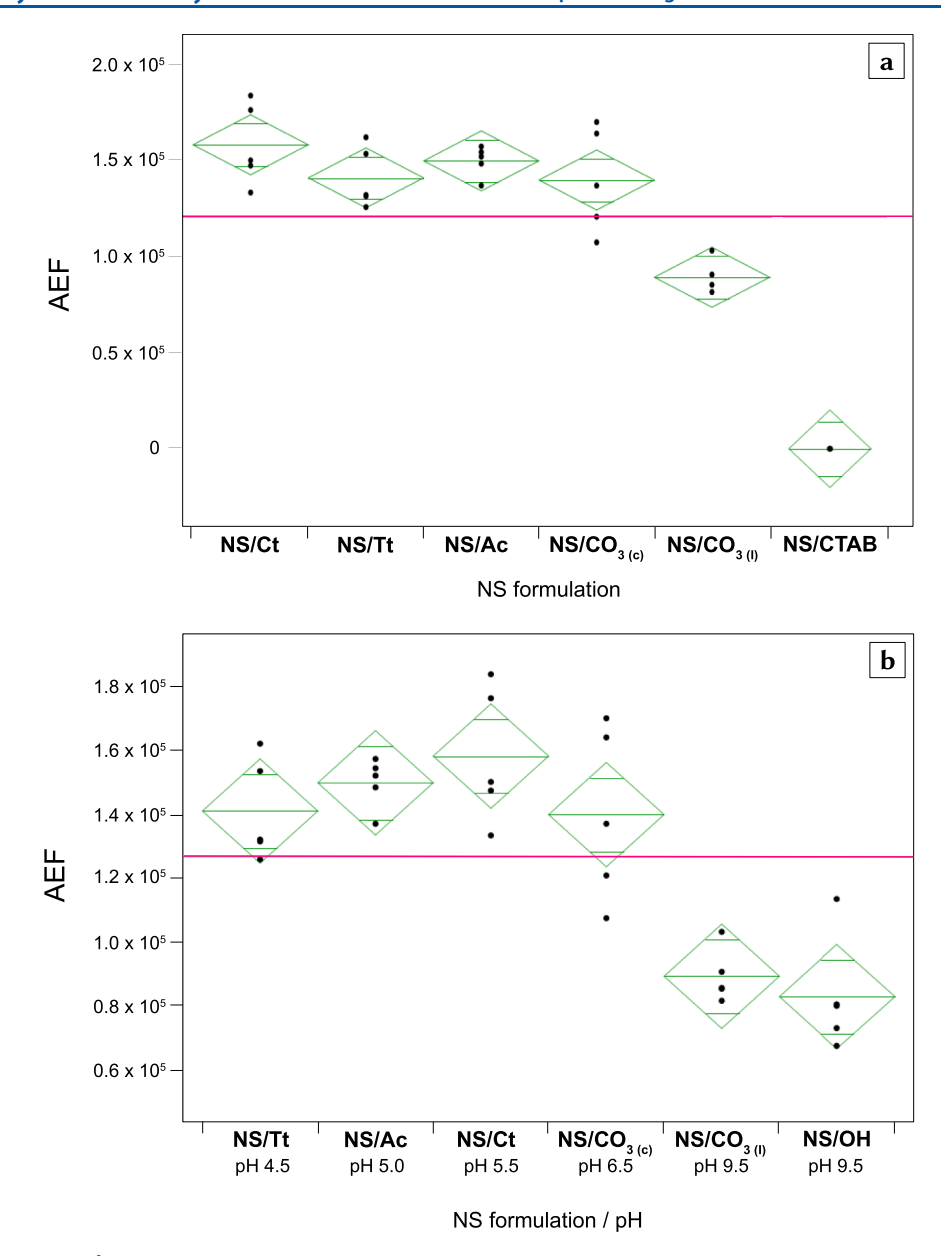


Figure 4. (a) ANOVA plot (R^2 0.9110) for the AEF values of the CV-NS systems under study. The pink horizontal line represents the global mean ($1.2 \pm 0.5 \times 10^5$), while the green rhomboids represent the quartiles relative to each sample group. (b) ANOVA plot (R^2 0.7766) for the AEF values of the CV-NS systems under study, compared to CV-NS/OH and ordered as a function of pH of the formulation. The pink horizontal line represents the global mean ($1.3 \pm 0.5 \times 10^5$), while the green rhomboids represent the quartiles relative to each sample group.

Table 3. Shelf Lives of the NS Formulations

formulation	estimated shelf life	
NS/Ct	<1 month	
Ns/Tt	<2 weeks	
NS/Ac	<1 month	
NS/CO ₃ ²⁻ (c) NS/CO ₃ ²⁻ (I)	≥4 months	
$NS/CO_3^{2-}(I)$	≈2 weeks	

Furthermore, the same formulation exhibited no statistically significant changes at both 1 and 4 months compared to its t_0 reference. For this reason, it was identified as the formulation with the longest shelf life among the studied array.

A detailed discussion of the results relative to NS/Ac and NS/CO_3^{2-} _(I) can be found in Section SN of the Supporting Information. The final stability can be formalized as follows

$$NS/Tt \ll NS/CO_3^{2-}_{(I)} < NS/Ac < NS/Ct$$

 $\ll NS/CO_3^{2-}_{(c)}$

The differences in shelf life among the various formulations were hypothesized to originate from differences in the $K_{\rm ad}$ between each capping agent and the metallic substrate and from differences in the ability of each capping agent to form an intermolecular network to further stabilize the capping crown. In the specific case of the two NS/CO₃²⁻ formulations, an additional reason could be identified in the higher conductivity of the NS/CO₃²⁻_(I) formulation compared to NS/CO₃²⁻_(c) (Table 1 and Figure S5). This is associated with compression of the electric double layer and thus coagulation. ⁶⁰

3.3. Part 3: Study of the Interaction Mode of the Stabilizers. The interaction between the model stabilizer

citrate and the bimetallic nanostar surface were studied by both ELS and Fourier transform infrared (FTIR) spectroscopy. FTIR spectroscopy was also utilized to study the remainder of the optimized formulations. While ELS measurements are typically utilized to assess the sign and extent of surface charging of a given system, they can also be utilized to extrapolate information regarding the strength of the interactions between a surface and associated charged species. Previously (Figure S2a), it was noted that the behavior of the ζ potential as a function of the concentration of the model stabilizer trisodium citrate resembles an adsorption isotherm. By fitting the experimental data points with a suitable, thermodynamically derived 61 adsorption model, the $K_{\rm ad}$ between the stabilizer and the AuAg surface and the change in free energy upon adsorption, ΔG_{ad} , can be estimated. A similar strategy has been utilized in SERS studies to estimate the strength of the interaction between the analyte and substrate. 62,63 Additionally, obtaining two ζ potential datasets at two different temperatures (10 °C, as a mild refrigeration condition, and 20 °C, as a room temperature condition), allows for recommendations regarding the most suitable storage conditions for the colloidal nanostars. A significantly higher adsorption constant at a colder temperature would indicate the suitability of storing the nanostar formulations under refrigeration, potentially increasing the shelf life.

Infrared spectroscopy can provide evidence of the nature of an adsorbate on a nanoparticle surface, also determining the type of coordination that a ligand adopts with respect to a surface. 64,65 In the specific case of carboxylates, it was noted by Deacon and Phillips⁶⁶ that the coordination chemistry of these compounds can be identified on the basis of the difference between the symmetric and asymmetric carbonyl stretching modes, $\Delta \nu (\text{COO}^-)$, as compared to that of the free, ionic carboxylate in solution. As a result of the observation of the IR spectra of a collection of formate and acetate complexes and correlation to their X-ray crystallographic structures, Deacon and Phillips were able to formulate guidelines for the assignment of the coordination modes of carboxylates: 66,67 Their $\Delta \nu (\text{COO}^-)$ trends have been demonstrated computationally to be the result of the changes in the COO- bond length and angle, which are valid also for compounds in aqueous solution. 67 Free, ionic carboxylates in solution are approximately symmetrical and have equidistant carbon—oxygen pairs. 64,67,68 However, upon unidentate coordination, the COO- functional group experiences a shortening of the carbonyl bond and a lengthening of the carboxyl bond (C-O of C-O···M), while upon bidentate coordination, the COOangle becomes narrower.67

3.3.1. ELS Titrations. When plotting the adsorption isotherms, possible contributions to the ζ potential from species other than citrate must be considered. As previously mentioned, the unmodified nanostars possess some surface charge. Even if this is insufficient to stabilize the colloidal sol, it must be taken into consideration when studying the effects of added species on the magnitude of the surface charge. Of the species that are present in solution, the most likely to contribute to the surface charge is Cl⁻ because it is known to interact with gold and silver. For example, the $\nu(Ag-Cl)$ band at around 240 cm⁻¹ is frequently observed in SERS spectra when utilizing hydroxylamine chloride-reduced Ag nanospheres, as they have a surface environment comprising chloride ions. ^{69,70} The same band is also observed when other Au or Ag colloidal systems are aggregated by the addition of

inorganic chloride salts such as NaCl or MgCl₂.⁷¹ Chloride species, however, have been reported to have weaker interactions with bulk and nanoscale gold, compared to citrate. 72,73 It should be noted that the bimetallic nanostars utilized in this research are primarily composed of gold (Au/ Ag = 18:1), and the surface charge of these (unmodified) nanostars is primarily caused by adsorbed chloride ions, derived from the reactant HAuCl₄. The first addition of citrate to such a colloidal sol may be expected to displace these chloride ions, and because of this, citrate is expected to cause an initial, not purely additive change in the magnitude of the ζ potential. Therefore, all ζ potential values were corrected by a factor corresponding to the lowest citrate titration point and plotted as a difference, $\Delta \zeta$. These differences represent the successive increases in surface charge upon addition of citrate, after initial displacement of chloride ions. Finally, the absolute value of these differences was taken, thus obtaining a set of positive responses, which allows the data to be fitted using common adsorption models.

In order to avoid a priori exclusion of cooperative adsorption and formation of ad-layers, the Hill expansion of the Langmuir model was chosen to fit the $\Delta |\zeta|$ data. The Hill—Langmuir model relies on the same assumptions of the pure Langmuir model, with the exception that cooperativity between adsorbate molecules is taken into account. According to the Hill expansion of the Langmuir model, cooperativity is fixed, indicating that it depends on the system and not on the adsorbate saturation conditions, and it can be modeled by an exponent, n, the Hill coefficient. In a system that obeys a pure Langmuir behavior, there is no cooperativity and n is equal to unity. Therefore, the adsorption can mathematically be described by the following expression $7^{4,75}$

$$\theta = \frac{y_i}{y_{\text{sat}}} = \frac{K_{\text{ad}}[\text{adsorbate}]_i^n}{1 + K_{\text{ad}}[\text{adsorbate}]_i^n} = \frac{[\text{adsorbate}]_i^n}{K_{\text{d}}[\text{adsorbate}]_i^n}$$
(10)

where $K_{\rm d}$ is the desorption constant expressed in M units, which is equal to $1/K_{\rm ad}$, both in value and thermodynamic meaning. The Hill coefficient n is greater than unity in situations in which the adsorption of a molecule favors the subsequent adsorption of other molecules (positive cooperativity), whether they are the same adsorbate species or not. On the other hand, when the adsorption of a molecule prevents or discourages further adsorption of species, the n coefficient is less than unity. The same adsorption of species and the same adsorption is less than unity.

If eq 10 is adapted to ζ potential terms, the Hill expansion of the Langmuir adsorption model becomes

$$\theta = \frac{\Delta |\zeta|_{i}}{\Delta |\zeta|_{\text{sat}}} = \frac{K_{\text{ad}}[\text{Ct}]_{i}^{n}}{1 + K_{\text{ad}}[\text{Ct}]_{i}^{n}} = \frac{[\text{Ct}]_{i}^{n}}{K_{\text{d}}[\text{Ct}]_{i}^{n}}$$
(11)

$$\Delta |\zeta|_{i} = \Delta |\zeta|_{\text{sat}} \frac{\left[\text{Ct}\right]_{i}^{n}}{K_{\text{d}}\left[\text{Ct}\right]_{i}^{n}} \tag{12}$$

which is the form that was utilized to fit the experimental data, at the two different temperatures of 10 and 20 °C, as shown in Figure 5. The Hill model demonstrated a good fit, with adjusted R^2 values of 0.9926 for the dataset at 10 °C and 0.9885 at 20 °C and χ_{ν}^2 values of 1.0742 and 1.0644 at 10 and 20 °C, respectively, and residual plots following a distribution close to normal at both temperatures (Figure S36 in the Supporting Information). The equations, whose parameters are summarized in Table 4, demonstrate the existence of a positive cooperativity among the adsorbate molecules, with a Hill

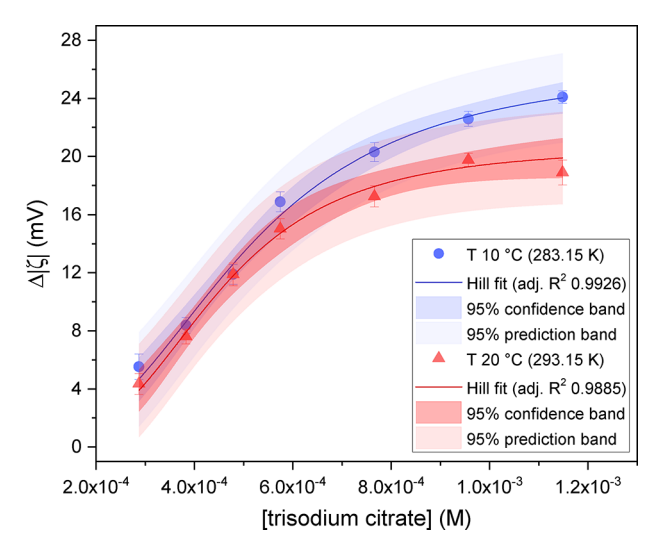


Figure 5. Plots of the change in the absolute value of the ζ potential, $\Delta |\zeta|$, as a function of increasing concentration of trisodium citrate, at 10 °C (blue dots) and 20 °C (red triangles). The data points were fitted to the Hill expansion of the Langmuir adsorption model (Equation 12).

Table 4. Fitting and Thermodynamic Parameters for the NS/Ct System, at 10 and 20 °C^a

parameter	10 °C	20 °C
adjusted R ²	0.9926	0.9885
$\chi_{ u}^{2}$	1.0742	1.0644
$\Delta \zeta_{sat} \ (mV)$	26 ± 1	20.6 ± 0.8
N	2.8 ± 0.3	3.4 ± 0.4
$K_{\rm d}$ (M)	$4.9 \pm 0.5 \times 10^{-4}$	$4.4 \pm 0.4 \times 10^{-4}$
$K_{\rm ad}~({ m M}^{-1})$	$2.0 \pm 0.3 \times 10^3$	$2.3 \pm 0.2 \times 10^3$
$K_{ m eq}$	$\approx 4.9 \pm 0.5 \times 10^{-4}$	$\approx 2.3 \pm 0.2 \times 10^3$
ΔG_{ad} (kcal/mol)	-4.36 ± 0.08	-4.58 ± 0.05

"The uncertainties of the $\Delta |\zeta_{\rm sat}|$ and n parameters correspond to the respective standard error; the uncertainties on the $K_{\rm d}$ values are the 95% confidence interval; all uncertainties of derived parameters are calculated using error propagation rules.

coefficient larger than 1 at both probed temperatures. An explanation of the positive cooperative binding of citrate onto the nanostars could be given by the establishment of hydrogen bonds among individual adsorbate molecules. This type of interaction has been reported to stabilize the multilayer citrate crown of traditional gold nanoparticles in a series of publications. 22,76-79 For example, Park and Shumaker-Parry 22 proposed a multilayer citrate network model held by hydrogen bonds and van der Waals forces to describe the capping environment of citrate-reduced gold nanospheres, and Wall et al. 76 proposed a similar hydrogen-bonded network with possible ad-layer formation. Although the nanostars are bimetallic and thus chemically different from pure gold nanoparticles, they are mostly composed of gold. For this reason, an interpretation of the adsorption cooperativity of citrate on AuAg nanostars in terms of hydrogen bonding seems reasonably justified by the literature cited above.

The $K_{\rm d}$ values were directly extrapolated from the Hill fit and were 4.9 \pm 0.5 \times 10⁻⁴ M at 10 °C and 4.4 \pm 0.4 \times 10⁻⁴ M at 20 °C, where the associated uncertainties were calculated as the two-tailed 95% confidence intervals. These values were then utilized to calculate the adsorption constants, $K_{\rm ad}$, which

were 2.0 \pm 0.3 \times 10³ M⁻¹ at 10 °C and 2.3 \pm 0.2 \times 10³ M⁻¹ at 20 °C

Another thermodynamic parameter that can be derived from the Hill isotherm is the change in the free energy of adsorption, $\Delta G_{\rm ad}$. Because the Hill model is an expansion of the Langmuir equation, the $K_{\rm ad}$ derived by it can be properly considered numerically equivalent to $K_{\rm eq}^{}$ such that

$$\Delta G = -RT \ln(K_{eq}) \approx -RT \ln[K_{ad}(1 \text{ M}^{-1})]$$
(13)

where R is the ideal gas constant (8.314 J × K⁻¹ × mol⁻¹; 0.001987 kcal × K⁻¹ × mol⁻¹) and T is the absolute temperature. This numerical equivalence allowed for the calculation of the $\Delta G_{\rm ad}$ at the two temperatures of 10 and 20 °C, which were -4.3 ± 0.1 and -4.58 ± 0.05 kcal/mol, respectively. This indicates a spontaneous process. When comparing the adsorption behavior at the two temperatures, the differences are not drastic, and a small increase in the magnitude of the adsorption is observed at the lower temperature. This trend might suggest two possibilities: the shelf life might not improve by storing the NS/Ct under refrigerated conditions and more interestingly, the mechanism driving the adsorption of citrate to the nanostar surface might be chemisorptive in nature.

An increase in the apparent adsorption capacity with increasing temperature can be associated with chemisorption.⁸¹ In this case, the chemisorption of citrate to the nanostars is likely weak because $K_{\rm ad}$ at both probed temperatures is around 10³ M⁻¹. This finding is consistent with that reported by Al-Johani et al. for another type of citrate-capped colloidal nanoparticle, ²¹ in which citrate is chemisorbed to an essentially neutral gold surface, via coordinating covalent bonding. The results obtained thus far for the bimetallic nanostars seem to suggest a similar trend, where the gold-silver surface is both alloyed and in its elemental oxidation state (XPS results, Section SD in the Supporting Information), and the carboxylate-based stabilizers interact with it via the formation of chemical bonds (ζ potential vs conductivity studies and extinction spectroscopy, Sections 3.2.1 and 3.2.2). For citrate, this adsorption process is likely the result of a weak chemisorption.

The $K_{\rm ad}$ in the order of $10^3~{\rm M}^{-1}$ calculated for citrate indicates an affinity that is 2 orders of magnitude lower than that reported for drugs of public health interest on plasmonic substrates (typically, $\approx 10^5 \text{ M}^{-1}$). 62,63 This makes citrate ideal for SERS applications involving analytes of similar structures, as it can be expected that they will be able to easily displace the citrate stabilizer and achieve a close contact with the enhancing substrate, thus yielding high-intensity SERS spectra. This statement should be taken into account with reasonable caution, as case-by-case specificities do play an important role in SERS experiments and the stabilizer might not be displaced in highly complex systems. Nevertheless, a highly characterized surface such as that of the NS/Ct formulation presented in this paper facilitates troubleshooting during the optimization of experimental conditions, leading to the implementation of robust analytical protocols.

3.3.2. FTIR Spectroscopy. As shown in Figure 6, the spectral profile of the purified and dried NS/Ct residue (blue line) shows two main bands at 1586 and 1396 cm⁻¹. These bands were assigned to the asymmetric and symmetric stretching modes of carboxylate, respectively, $\nu_{\rm as}({\rm COO}^-)$ and $\nu_{\rm s}({\rm COO}^-)$. Compared to the spectrum obtained from drop-casting

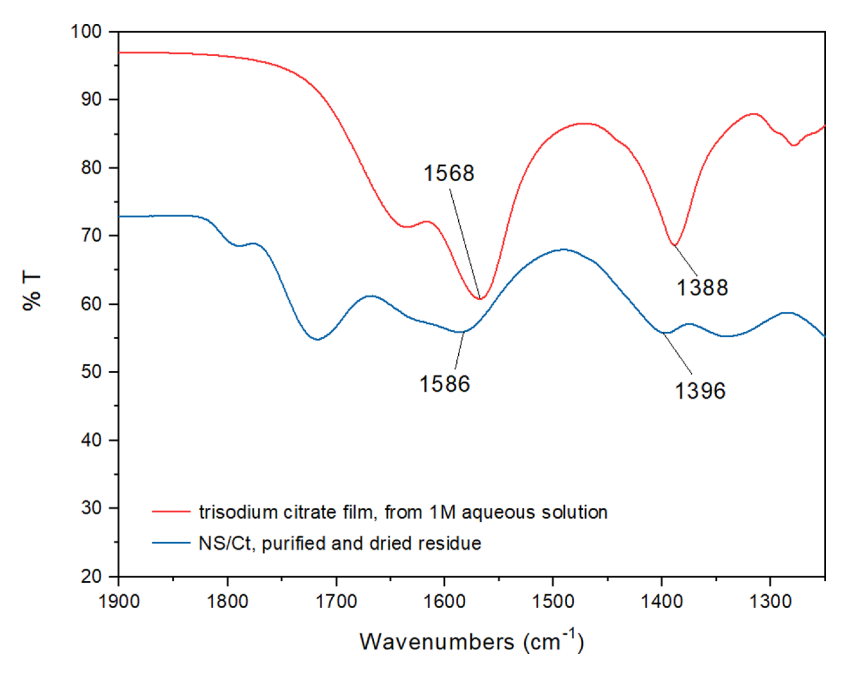


Figure 6. FT-IR ATR spectra of the free citrate ion (top, red), obtained by drop-casting a 1 M trisodium citrate solution on the IRE, and of the purified and dried NS/Ct residues (bottom, blue). Spectra are on the same scale but stacked for ease of comparison.

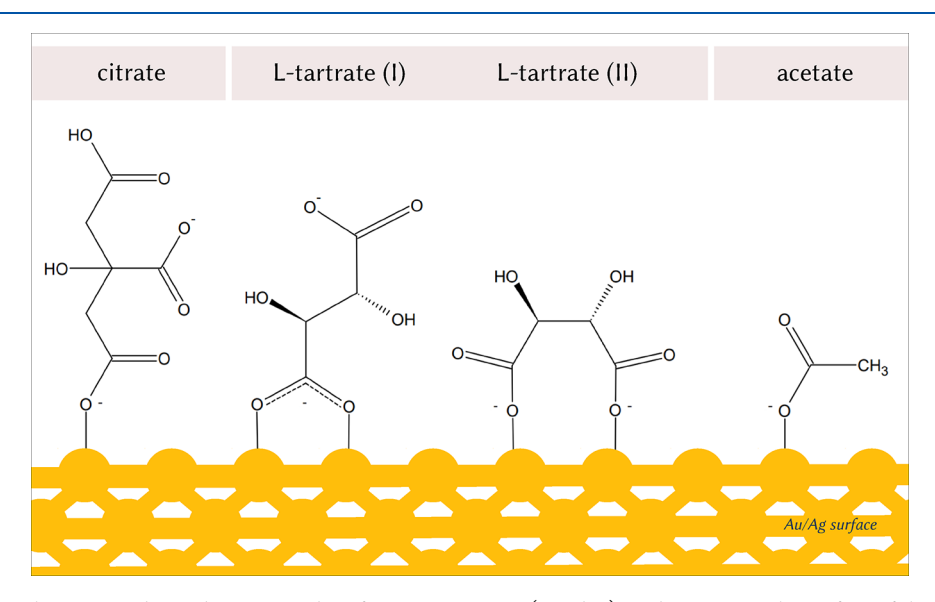


Figure 7. From left to right, proposed coordination modes of citrate, L-tartrate (I and II), and acetate on the surface of the nanostars. The species are represented as their most abundant charged species.

aqueous trisodium citrate onto the IRE (top, red line in Figure 6), the $\nu_{\rm as}({\rm COO^-})$ band shows a shift of 18 cm⁻¹ toward higher wavenumbers. This is typically observed in carboxylates that experience an asymmetric change in the bond length of the COO⁻ group, such as those forming a unidentate complex with a metal. ^{65,66,82} This results in a shift of the $\nu_{\rm as}({\rm COO^-})$ band at higher wavenumbers ($\approx \nu_{\rm as}({\rm C=O})$) and of the $\nu_{\rm s}({\rm COO^-})$ band at slightly lower wavenumbers ($\approx \nu_{\rm as}({\rm C-O})$), ⁸² compared to the free, ionic citrate. These shifts ultimately result in the $\Delta\nu({\rm COO^-})$ trends described by Deacon and Phillips for unidentate coordination complexes. ^{65–67} Since the calculated $\Delta\nu({\rm COO^-})$ for the free ion is 180 cm⁻¹, while the $\Delta\nu({\rm COO^-})$ for the NS/Ct residue is 190 cm⁻¹, the citrate can be inferred to be interacting with the bimetallic surface by forming a unidentate coordinate covalent

bond with it. This binding mode is in accordance with the concentration—coordination relationship trends highlighted by Al-Johani et al. via solid-state NMR measurements. At low concentrations, citrate interacted with the gold surface with the bridging coordination mode and then switched to the bidentate mode with increasing concentration and finally to the unidentate mode when the surface coverage was near saturation. On the basis of the ζ titration results, the concentration used to prepare the NS/Ct formulation was near the [Ct]_{sat} for the system. The $\Delta\nu(\text{COO}^-)$ value observed for NS/Ct is also in accordance with the hypothesis of hydrogen bonding among the different citrate units that was formulated as a result of the ζ titration experiments. Deacon and Phillips report that unidentate coordination complexes of carboxylates with $\Delta\nu(\text{COO}^-)$ values lower than 200 cm⁻¹

are associated with hydrogen bonding interactions between the noncoordinating C–O (\approx C=O) and other species that might be present in the system.

The same procedure was replicated for the NS/Tt and NS/ Ac formulations, and a detailed interpretation of their spectra (Figures S37 and S38) is reported in Section SP in the Supporting Information. Briefly, the NS/Tt formulation was hypothesized to have a population of differently coordinated tartrate molecules, namely undergoing bridging and doubleunidentate bridging coordination, while acetate in the NS/Ac residue was found to interact in a unidentate fashion (Figure 7). The $NS/CO_3^{\ 2-}{}_{(I)}$ formulation was also analyzed by the same methodology, but it did not yield any significant spectral information. The absence of observable carbonate bands could be caused by an undetectable concentration of the species, such that $[CO_3^{2-}]_{surface} < LOD_{CO_3^{2-}}$, which would suggest that the main stabilizing species on the nanostars' surface are in fact hydroxyl ions, which are generated in solution by carbonate. In this case, hydroxyl vibrations would be undistinguishable from the background signal, and thus, this hypothesis cannot be verified by the analytical protocol discussed here.

4. CONCLUSIONS

SERS is a surface spectroscopic technique that relies on the adsorption of analytes to nanoscale plasmonic substrates enabling trace and ultratrace detection. When colloidal substrates are utilized, knowledge of the adsorption phenomena at the nanoscale is an essential tool for the rational design of substrates and the development of detection protocols tailored for specific classes of molecules. While great emphasis has been posed on analyte-substrate interactions, the literature on the stabilizer-substrate interactions is far less developed. For example, what drives the plasmonic nanoparticle capping process and how is this affected by the oxidation state of the plasmonic nanoparticle? What are the interactions between capping agents and plasmonic surfaces and how can this knowledge be exploited to fabricate tailored substrates for SERS applications? Lastly, is the capping environment critical to achieving low limits of detection? The present work is aimed at addressing these fundamental questions by developing an array of colloidally stable bimetallic gold-silver nanostar formulations and systematically studying their optical properties, SERS performance, and shelf life. This included characterization of the morphology and chemical composition of the nanoparticles and the adsorption modes of capping agents on the metallic surface.

We utilized a protocol for the synthesis of sparingly capped colloidal nanostars 17,28 to provide a platform for investigating the stabilizing properties of a selection of small anionic molecules and to examine their behavior with respect to surface adsorption and SERS performance. Among the surveyed species, the small anions that were found to achieve colloidal stability were citrate, L-tartrate, acetate, and carbonate sodium salts. The remaining organic and inorganic anionic species that were surveyed (sodium sulfite, sulfate, nitrate, and 1,3-propanedisulfonic acid disodium salt) did not demonstrate stabilization properties, thus supporting our hypothesis that the capping process is driven by chemisorption, that is, an adsorption that occurs via the formation of chemical bonds. Surface characterization by XPS also supported the chemisorption hypothesis, as it showed that the two metals constituting the nanostars, gold and silver, are alloyed and in

their elemental oxidation state. Chemically driven adsorption of species at the solid/liquid interface is therefore a reasonable explanation for the capping process and the ensuing surface charge on the nanostars. These findings are consistent with recent studies, such as those published by Al-Johani et al., who determined a similar oxidation state for monometallic gold nanospheres. Therefore, our results can be thought of as an extension of their conclusions to bimetallic systems and contribute to a better understanding of the chemistry of the surface of colloidal noble metal nanoparticles. This is often depicted bearing a residual positive charge, 83,84 which the experimental evidence herein refutes.

A novel methodology for determining the shelf life was developed. Results indicated that the shelf life is mainly dependent on the adsorptive properties of the stabilizer. This was hypothesized to be the result of differences between each stabilizer—alloy $K_{\rm ad}$, the ability of the stabilizer to form an intermolecular network, and differences in the conductivity of the formulation.

All new formulations were characterized in terms of optical and morphological reproducibility and were demonstrated to achieve superior (i.e., 2 orders of magnitude higher) SERS performance compared to the original formulation which utilized CTAB as a stabilizer. Although these foundational experiments were all conducted utilizing CV as an ideal SERS probe, the superiority in performance was also verified with nonideal probes, such as the opioids acrylfentanyl and benzylfentanyl (Supporting Information). Moreover, the NS/ CO₃²⁻(c) formulation has already been successfully applied to the detection of such a class of analytes, both in standard solutions⁸⁵ and in binary mixtures of other abused substances.⁸⁶ While the effects of nanoparticle morphology are commonly reported in the literature, comparisons of different surface environments are less frequently explored. In our case, the effect of the surface environment was deemed more important than that of shape, encouraging further exploration of surface chemistry in the optimization of SERS-based analytical protocols.

Citrate was selected as the model stabilizer, and the energetics of its adsorption on the nanostars were studied via ELS titrations. To the best of our knowledge, this is the first time an ELS-based method is reported for the study of thermodynamic quantities of adsorbed species on noble metal nanoparticles. The ELS titration experiments demonstrated that citrate caps the nanoparticles by weak chemisorption, in line with previous publications on monometallic gold nanoparticles.²¹ In addition, this weak chemisorption was found to be characterized by positive cooperativity. Future work will entail exploring the nature of this positive cooperativity via theoretical studies based on DFT.

Finally, the coordination mode of citrate (unidentate), L-tartrate (bridging), and acetate (unidentate) on the bimetallic surface was deduced by the examination of dried residues of their respective NS formulations by FTIR spectroscopy.

Overall, this research offers an example of how characterization of surface chemistry can be a great aid in the understanding of SERS and in formulating tailored nanomaterials for rational protocol design. This approach has the potential of developing surface chemistry that can be straightforwardly applied in subsequent protocol development, thus extending the range of applicability of SERS as a routine analytical technique. Ongoing and future advancements of this work may include more extensive application of colloidal

nanostars. For example, they can be used to implement an analytical protocol for the SERS detection of novel psychoactive substances in toxicological samples. Moreover, the general scheme utilized for the characterization and engineering of the surface environment of the nanostars could be adopted as a basis for further development and functionalization of a wide variety of colloidal nanomaterials.

ASSOCIATED CONTENT

Supporting Information

The Supporting Information is available free of charge at https://pubs.acs.org/doi/10.1021/acs.jpcc.1c08145.

Figures S1 to S38 and Description of the as-synthesized nanostars; additional information on the optimization of the colloidal formulations; surface characterization of NS/Ct by XPS; TEM micrographs of NS/Tt, NS/Ac, NS/CO₃²⁻_(c), and NS/CO₃²⁻_(l); extinction spectroscopy: examples of stable and unstable formulations; characterization of CV; evolution of the intensity profile over time; reaction scaling-up; reproducibility of optical properties and effects on SERS intensity; morphological characterization: variability and yield; importance of the surface environment; AEF; shelf life determination; zeta potential titrations; and FTIR spectroscopy (PDF)

AUTHOR INFORMATION

Corresponding Author

Bruce McCord — Department of Chemistry and Biochemistry, Florida International University, Miami, Florida 33199, United States; orcid.org/0000-0002-8366-1925; Phone: +1 (305) 348-7543; Email: mccordb@fiu.edu

Authors

Chiara Deriu – Department of Chemistry and Biochemistry, Florida International University, Miami, Florida 33199, United States

Asier Bracho – Department of Chemistry and Biochemistry, Florida International University, Miami, Florida 33199, United States

Complete contact information is available at: https://pubs.acs.org/10.1021/acs.jpcc.1c08145

Notes

The authors declare no competing financial interest.

ACKNOWLEDGMENTS

The authors would like to acknowledge Eric Lambers (University of Florida, Gainesville, FL) for performing the XPS measurements, Dr. Alexander Franco Hernandez (AMERI, Florida International University, Miami, FL) for performing the TEM analysis, and Dr. Yong Cai (Florida International University, Miami, FL) for access to ELS equipment. Measurements of fentanyl analogs were made possible by NSF IUCRC award 1739805 to Florida International University—Center for Advanced Research in Forensic Science (FIU-CARFS), while TEM analysis was made possible by the IFRI Student Development Award 2020. The rest of this research did not receive any specific grant from funding agencies in the public, commercial, or not-for-profit sectors. C.D. would also like to acknowledge the University Graduate School (UGS) at Florida International University for the

Dissertation Year Fellowship award received for the Fall 2020 semester.

REFERENCES

- (1) Smith, E.; Dent, G. Modern Raman Spectroscopy, a Practical Approach, 2nd ed.; John Wiley & Sons Ltd.: Chichester, 2019.
- (2) Le Ru, E. C.; Etchegoin, P. G. Principles of Surface-Enhanced Raman Spectroscopy and Related Plasmonic Effects; Elsevier: Amsterdam, 2009.
- (3) Kneipp, K.; Wang, Y.; Kneipp, H.; Perelman, L. T.; Itzkan, I.; Dasari, R. R.; Feld, M. S. Single Molecule Detection Using Surface-Enhanced Raman Scattering (SERS). *Phys. Rev. Lett.* **1997**, 78, 1667—1670
- (4) Kneipp, K.; Kneipp, H.; Bohr, H. G. Single-Molecule SERS Spectroscopy. In *Surface Enhanced Raman Scattering*; Kneipp, K., Moskovits, M., Kneipp, H., Eds.; Springer-Verlag: Berlin Heidelberg, 2006
- (5) Pilot, R.; Signorini, R.; Durante, C.; Orian, L.; Bhamidipati, M.; Fabris, L. A Review on Surface-Enhanced Raman Scattering. *Biosensors* **2019**, *9*, 57.
- (6) Moskovits, M. Persistent Misconceptions Regarding SERS. *Phys. Chem. Chem. Phys.* **2013**, *15*, 5301–5311.
- (7) Everett, D. H. Basic Principles of Colloid Science, 1st ed.; RSC Paperbacks; Royal Society of Chemistry: Cambridge, 1988.
- (8) David Fermina, D.; Riley, J. Charge in Colloidal Systems. In *Colloid Science Principles, methods and applications*; Cosgrove, T., Ed.; Wiley: Chichester, 2010; pp 23–43.
- (9) Murphy, C. J.; Buriak, J. M. Best Practices for the Reporting of Colloidal Inorganic Nanomaterials. *Chem. Mater.* **2015**, *27*, 4911–4913.
- (10) Sivapalan, S. T.; DeVetter, B. M.; Yang, T. K.; van Dijk, T.; Schulmerich, M. V.; Carney, P. S.; Bhargava, R.; Murphy, C. J. Off-Resonance Surface-Enhanced Raman Spectroscopy from Gold Nanorod Suspensions as a Function of Aspect Ratio: Not What We Thought. ACS Nano 2013, 7, 2099–2105.
- (11) Alvarez-Puebla, R. A.; Liz-Marzán, L. M. Traps and Cages for Universal SERS Detection. *Chem. Soc. Rev.* **2012**, *41*, 43–51.
- (12) Haynes, C. L.; Haes, A. J.; McFarland, A. D.; Van Duyne, R. P. Nanoparticles with Tunable Localized Surface Plasmon Resonances. In *Topics in Fluorescence Spectroscopy*; Gedde, C. D., Lakowicz, J. R., Eds.; Springer Science + Business Media Inc.: New York, 2005; pp 47–99.
- (13) Lee, K.-S.; El-Sayed, M. A. Gold and Silver Nanoparticles in Sensing and Imaging: Sensitivity of Plasmon Response to Size, Shape, and Metal Composition. *J. Phys. Chem. B* **2006**, *110*, 19220–19225.
- (14) Gellner, M.; Küstner, B.; Schlücker, S. Optical Properties and SERS Efficiency of Tunable Gold/Silver Nanoshells. *Vib. Spectrosc.* **2009**, *50*, 43–47.
- (15) Liu, X.-L.; Wang, J.-H.; Liang, S.; Yang, D.-J.; Nan, F.; Ding, S.-J.; Zhou, L.; Hao, Z.-H.; Wang, Q.-Q. Tuning Plasmon Resonance of Gold Nanostars for Enhancements of Nonlinear Optical Response and Raman Scattering. *J. Phys. Chem. C* **2014**, *118*, 9659–9664.
- (16) Webb, J. A.; Erwin, W. R.; Zarick, H. F.; Aufrecht, J.; Manning, H. W.; Lang, M. J.; Pint, C. L.; Bardhan, R. Geometry-Dependent Plasmonic Tunability and Photothermal Characteristics of Multibranched Gold Nanoantennas. *J. Phys. Chem. C* **2014**, *118*, 3696–3707
- (17) He, S.; Kang, M. W. C.; Khan, F. J.; Tan, E. K. M.; Reyes, M. A.; Kah, J. C. Y. Optimizing Gold Nanostars as a Colloid-Based Surface-Enhanced Raman Scattering (SERS) Substrate. *J. Opt.* **2015**, *17*, 114013–114026.
- (18) De Silva Indrasekara, A. S.; Johnson, S. F.; Odion, R. A.; Vo-Dinh, T. Manipulation of the Geometry and Modulation of the Optical Response of Surfactant-Free Gold Nanostars: A Systematic Bottom-Up Synthesis. *ACS Omega* **2018**, *3*, 2202–2210.
- (19) Harder, R. A.; Wijenayaka, L. A.; Phan, H. T.; Haes, A. J. Tuning Gold Nanostar Morphology for the SERS Detection of Uranyl. *J. Raman Spectrosc.* **2021**, *52*, 497–505.

- (20) Alvarez-Puebla, R. A.; Arceo, E.; Goulet, P. J. G.; Garrido, J. J.; Aroca, R. F. Role of Nanoparticle Surface Charge in Surface-Enhanced Raman Scattering. *J. Phys. Chem. B* **2005**, *109*, 3787–3792. (21) Al-Johani, H.; Abou-Hamad, E.; Jedidi, A.; Widdifield, C. M.; Viger-Gravel, J.; Sangaru, S. S.; Gajan, D.; Anjum, D. H.; Ould-Chikh, S.; Hedhili, M. N.; et al. The Structure and Binding Mode of Citrate in the Stabilization of Gold Nanoparticles. *Nat. Chem.* **2017**, *9*, 890–895.
- (22) Park, J.-W.; Shumaker-Parry, J. S. Structural Study of Citrate Layers on Gold Nanoparticles: Role of Intermolecular Interactions in Stabilizing Nanoparticles. *J. Am. Chem. Soc.* **2014**, *136*, 1907–1921.
- (23) Wijenayaka, L. A.; Ivanov, M. R.; Cheatum, C. M.; Haes, A. J. Improved Parametrization for Extended Derjaguin, Landau, Verwey, and Overbeek Predictions of Functionalized Gold Nanosphere Stability. *J. Phys. Chem. C* 2015, *119*, 10064–10075.
- (24) Xi, W.; Phan, H. T.; Haes, A. J. How to Accurately Predict Solution-Phase Gold Nanostar Stability. *Anal. Bioanal. Chem.* **2018**, 410, 6113–6123.
- (25) Phan, H. T.; Haes, A. J. What Does Nanoparticle Stability Mean? *J. Phys. Chem. C* **2019**, 123, 16495–16507.
- (26) Xi, W.; Haes, A. J. Elucidation of HEPES Affinity to and Structure on Gold Nanostars. J. Am. Chem. Soc. 2019, 141, 4034–4042
- (27) Xie, J.; Lee, J. Y.; Wang, D. I. C. Seedless, Surfactantless, High-Yield Synthesis of Branched Gold Nanocrystals in HEPES Buffer Solution. *Chem. Mater.* **2007**, *19*, 2823–2830.
- (28) Cheng, L.-C.; Huang, J.-H.; Chen, H. M.; Lai, T.-C.; Yang, K.-Y.; Liu, R.-S.; Hsiao, M.; Chen, C.-H.; Her, L.-J.; Tsai, D. P. Seedless, Silver-Induced Synthesis of Star-Shaped Gold/Silver Bimetallic Nanoparticles as High Efficiency Photothermal Therapy Reagent. *J. Mater. Chem.* 2012, 22, 2244–2253.
- (29) Hunter, R. J. Foundations of Colloid Science, 2nd ed.; Oxford University Press: New York, 2001.
- (30) Israelachvili, J. N. Intermolecular and Surface Forces, 2nd ed.; Academic Press Inc.: San Diego, 1992.
- (31) Derjaguin, B. V.; Churaev, N. V.; Muller, V. M. Surface Forces; Springer US: Boston, MA, 1987.
- (32) Verwey, E. J. W. Theory of the Stability of Lyophobic Colloids. *J. Phys. Colloid Chem.* **1947**, *51*, 631–636.
- (33) Verwey, E. J.; Overbeek, J. T. G. Theory of the Stability of Lyophobic Colloids; Dover Publications: Mineola, NY, 1999.
- (34) Dukhin, A. S.; Goetz, P. J. Fundamentals of Interface and Colloid Science. In *Characterization of Liquids, Dispersions, Emulsions, and Porous Materials Using Ultrasound*; Elsevier: Amsterdam, 2017; pp 19–83.
- (35) The International Association for the Properties of Water and Steam (IAPWS). Release on the IAPWS Formulation 2008 for the Viscosity of Ordinary Water Substance: Berlin, Germany, 2008.
- (36) Malmberg, C. G.; Maryott, A. A. Dielectric Constant of Water from 0° to 100°C. J. Res. Natl. Bur. Stand. 1956, 56, 1.
- (37) Bashkatov, A. N.; Genina, E. A. Water Refractive Index in Dependence on Temperature and Wavelength: A Simple Approximation. Proceedings of SPIE Vol. 5068, Laser Physics and Photonics, Spectroscopy, and Molecular Modeling III; Coherent Optics of Ordered and Random Media III, Fall 2002; Tuchin, V. V., Ed.; Society of Photo-Optical Instrumentation Engineers (SPIE): Saratov, Russian Federation, 2003; pp 393–395.
- (38) Malvern. Zetasizer Nano Series, User Manual; Malvern Instruments Ltd.: Worcestershire, U.K., 2013.
- (39) Henry, D. C. The Cataphoresis of Suspended Particles. Part I.The Equation of Cataphoresis. *Proc. R. Soc. London, Ser. A* 1931, 133, 106–129.
- (40) Delgado, A. V.; González-Caballero, F.; Hunter, R. J.; Koopal, L. K.; Lyklema, J. Measurement and Interpretation of Electrokinetic Phenomena. *Pure Appl. Chem.* **2005**, *77*, 1753–1805.
- (41) Ohshima, H. A Simple Expression for Henry's Function for the Retardation Effect in Electrophoresis of Spherical Colloidal Particles. *J. Colloid Interface Sci.* **1994**, *168*, 269–271.

- (42) Schneider, C. A.; Rasband, W. S.; Eliceiri, K. W. NIH Image to ImageJ: 25 Years of Image Analysis. *Nat. Methods* **2012**, *9*, 671–675.
- (43) Shnoudeh, A. J.; Hamad, I.; Abdo, R. W.; Qadumii, L.; Jaber, A. Y.; Surchi, H. S.; Alkelany, S. Z. Synthesis, Characterization, and Applications of Metal Nanoparticles. In *Biomaterials and Bionanotechnology, Advances in Pharmaceutical Product Development and Research Series*; Tekade, R. K., Ed.; Academic Press: London, 2019.
- (44) Wulandari, P.; Nagahiro, T.; Michioka, K.; Tamada, K.; Ishibashi, K.-i.; Kimura, Y.; Niwano, M. Coordination of Carboxylate on Metal Nanoparticles Characterized by Fourier Transform Infrared Spectroscopy. *Chem. Lett.* **2008**, *37*, 888–889.
- (45) Sonntag, H.; Strenge, K. Coagulation Kinetics and Structure Formation; Springer Science + Business Media: New York, 1987.
- (46) Sprycha, R.; Matijevic, E. Electrokinetics of Uniform Colloidal Dispersions of Chromium Hydroxide. *Langmuir* **1989**, *5*, 479–485.
- (47) Liu, Y.; Yan, E. C. Y.; Zhao, X.; Eisenthal, K. B. Surface Potential of Charged Liposomes Determined by Second Harmonic Generation. *Langmuir* **2001**, *17*, 2063–2066.
- (48) Giles, C. H.; MacEwan, T. H.; Nakhwa, S. N.; Smith, D. 786. Studies in adsorption. Part XI. A system of classification of solution adsorption isotherms, and its use in diagnosis of adsorption mechanisms and in measurement of specific surface areas of solids. *J. Chem. Soc.* **1960**, 3973–3993.
- (49) Giles, C. H.; Smith, D.; Huitson, A. A General Treatment and Classification of the Solute Adsorption Isotherm. I. Theoretical. *J. Colloid Interface Sci.* **1974**, *47*, 755–765.
- (50) O'Brien, R. W. The Solution of the Electrokinetic Equations for Colloidal Particles with Thin Double Layers. *J. Colloid Interface Sci.* 1983, 92, 204–216.
- (51) Ohshima, H. Electrical Conductivity of a Concentrated Suspension of Spherical Colloidal Particles. *J. Colloid Interface Sci.* 1999, 212, 443–448.
- (52) Goodacre, R.; Graham, D.; Faulds, K. Recent Developments in Quantitative SERS: Moving towards Absolute Quantification. *TrAC, Trends Anal. Chem.* **2018**, *102*, 359–368.
- (53) LeRu, E. C.; Etchegoin, P. Principles of Surface-Enhanced Raman Spectroscopy; Elsevier: Amsterdam, 2009.
- (54) Liu, S.; Ishimoto, T.; Koyama, M. First-Principles Calculation of OH-/OH Adsorption on Gold Nanoparticles. *Int. J. Quantum Chem.* **2015**, *115*, 1597–1605.
- (55) Santiago-Rodríguez, Y.; Herron, J. A.; Curet-Arana, M. C.; Mavrikakis, M. Atomic and Molecular Adsorption on Au(111). *Surf. Sci.* **2014**, *627*, 57–69.
- (56) Cañamares, M. V.; Chenal, C.; Birke, R. L.; Lombardi, J. R. DFT, SERS, and Single-Molecule SERS of Crystal Violet. *J. Phys. Chem. C* 2008, *112*, 20295–20300.
- (57) Zhou, L.; Zhou, J.; Lai, W.; Yang, X.; Meng, J.; Su, L.; Gu, C.; Jiang, T.; Pun, E. Y. B.; Shao, L.; et al. Irreversible Accumulated SERS Behavior of the Molecule-Linked Silver and Silver-Doped Titanium Dioxide Hybrid System. *Nat. Commun.* **2020**, *11*, 1785.
- (58) Le Ru, E. C.; Blackie, E.; Meyer, M.; Etchegoin, P. G.; Blackie, E. Surface Enhanced Raman Scattering Enhancement Factors: A Comprehensive Study. *J. Phys. Chem. C* **2007**, *111*, 13794–13803.
- (59) Beach, S. F.; Hepworth, J. D.; Mason, D.; Swarbrick, E. A. A Kinetic Study of the Hydrolysis of Crystal Violet and Some Terminal and Bridged Analogues. *Dyes Pigm.* **1999**, *42*, 71–77.
- (60) Atkins, P.; de Paula, J.; Keeler, J. Atkins' Physical Chemistry, 11th ed.; Oxford University Press: Oxford, 2018.
- (61) Liu, Y. Is the Free Energy Change of Adsorption Correctly Calculated? *J. Chem. Eng. Data* **2009**, *54*, 1981–1985.
- (62) Izquierdo-Lorenzo, I.; Sanchez-Cortes, S.; Garcia-Ramos, J. V. Adsorption of Beta-Adrenergic Agonists Used in Sport Doping on Metal Nanoparticles: A Detection Study Based on Surface-Enhanced Raman Scattering. *Langmuir* **2010**, *26*, 14663–14670.
- (63) Deriu, C.; Conticello, I.; Mebel, A. M.; McCord, B. Micro Solid Phase Extraction Surface-Enhanced Raman Spectroscopy (μ-SPE/SERS) Screening Test for the Detection of the Synthetic Cannabinoid JWH-018 in Oral Fluid. *Anal. Chem.* **2019**, *91*, 4780–4789.

- (64) Colthup, N. B.; Daly, L. H.; Wiberley, S. E. Introduction to Infrared and Raman Spectroscopy, 3rd ed.; Academic Press: Boston, 1990
- (65) Nakamoto, K. Infrared and Raman Spectra of Inorganic and Coordination Compounds. Part B: Applications in Coordination, Organometallic, and Bioinorganic Chemistry, 6th ed.; John Wiley & Sons: Hoboken, 2009.
- (66) Deacon, G.; Phillips, R. J. Relationships between the Carbon-Oxygen Stretching Frequencies of Carboxylato Complexes and the Type of Carboxylate Coordination. *Coord. Chem. Rev.* **1980**, 33, 227–250.
- (67) Sutton, C. C. R.; da Silva, G.; Franks, G. V. Modeling the IR Spectra of Aqueous Metal Carboxylate Complexes: Correlation between Bonding Geometry and Stretching Mode Wavenumber Shifts. Chem.—Eur. J. 2015, 21, 6801–6805.
- (68) Palacios, E. G.; Juárez-López, G.; Monhemius, A. J. Infrared Spectroscopy of Metal Carboxylates: II. Analysis of Fe(III), Ni and Zn Carboxylate Solutions. *Hydrometall* **2004**, *72*, 139–148.
- (69) Leopold, N.; Lendl, B. A New Method for Fast Preparation of Highly Surface-Enhanced Raman Scattering (SERS) Active Silver Colloids at Room Temperature by Reduction of Silver Nitrate with Hydroxylamine Hydrochloride. *J. Phys. Chem. B* **2003**, 107, 5723–5727
- (70) Dong, X.; Gu, H.; Liu, F. Study of the Surface-Enhanced Raman Spectroscopy of Residual Impurities in Hydroxylamine-Reduced Silver Colloid and the Effects of Anions on the Colloid Activity. *Spectrochim. Acta, Part A* **2012**, *88*, 97–101.
- (71) Sánchez-Cortés, S.; García-Ramos, J. V. Influence of Coverage in the Surface-Enhanced Raman Scattering of Cytosine and Its Methyl Derivatives on Metal Colloids: Chloride and PH Effects. *Surf. Sci.* **2001**, *473*, 133–142.
- (72) Thompson, D. W.; Collins, I. R. Electrical Properties of the Gold-Aqueous Solution Interface. *J. Colloid Interface Sci.* **1992**, *152*, 197–204.
- (73) Biggs, S.; Mulvaney, P.; Zukoski, C. F.; Grieser, F. Study of Anion Adsorption at the Gold-Aqueous Solution Interface by Atomic Force Microscopy. *J. Am. Chem. Soc.* **1994**, *116*, 9150–9157.
- (74) Hill, A. V. The Possible Effects of the Aggregation of the Molecules of Hemoglobin on Its Dissociation Curves. *J. Physiol.* **1910**, 40, 4–7.
- (75) Stefan, M. I.; Le Novère, N. Cooperative Binding. PLoS Comput. Biol. 2013, 9, No. e1003106.
- (76) Wall, J. F.; Grieser, F.; Zukoski, h. F. Monitoring Chemical Reactions at the Gold/Solution Interface Using Atomic Force Microscopy. J. Chem. Soc., Faraday Trans. 1997, 93, 4017–4020.
- (77) Lee, Z.; Jeon, K.-J.; Dato, A.; Erni, R.; Richardson, T. J.; Frenklach, M.; Radmilovic, V. Direct Imaging of Soft—Hard Interfaces Enabled by Graphene. *Nano Lett.* **2009**, *9*, 3365–3369.
- (78) Wright, L. B.; Rodger, P. M.; Walsh, T. R. Structure and Properties of Citrate Overlayers Adsorbed at the Aqueous Au(111) Interface. *Langmuir* **2014**, *30*, 15171–15180.
- (79) Perfilieva, O. A.; Pyshnyi, D. V.; Lomzov, A. A. Molecular Dynamics Simulation of Polarizable Gold Nanoparticles Interacting with Sodium Citrate. *J. Chem. Theory Comput.* **2019**, *15*, 1278–1292.
- (80) Ghosal, P. S.; Gupta, A. K. Determination of Thermodynamic Parameters from Langmuir Isotherm Constant-Revisited. *J. Mol. Liq.* **2017**, 225, 137–146.
- (81) IUPAC; Physical Chemistry Division; Commission on Colloid and Surface Chemistry Including Catalysis. Chemisorption and Physisorption. In *Definitions, Terminology and Symbols in Colloid and Surface Chemistry*, Internet Edition; Elsevier Science, 2001. Originally Everett, D.H. Manual of Symbols and Terminology for Physicochemical Quantities and Units, Appendix II: Definitions, Terminology and Symbols in Colloid and Surface Chemistry. Pure Appl. Chem. 1972, 31 (4), 579–638.
- (82) Dresseyn, H. O. Vibrational Analysis of Acid Derivatives. In The Chemistry of Acid Derivatives, The Chemistry of Functional Groups, Supplement B, Vol. 2; Patai, S., Ed.; Wiley: Chichester, 1992.

- (83) Aroca, R. Surface-Enhanced Vibrational Spectroscopy; John Wiley & Sons, Ltd: Chichester, U.K., 2006.
- (84) Mulvaney, P. Metal Nanoparticles: Double Layers, Optical Properties, and Electrochemistry. In *Nanoscale Materials in Chemistry*; Klabunde, K. J., Ed.; John Wiley & Sons, Inc.: New York, USA, 2021; pp 121–167.
- (85) Wang, L.; Deriu, C.; Wu, W.; Mebel, A. M.; McCord, B. Surface-enhanced Raman spectroscopy, Raman, and density functional theoretical analyses of fentanyl and six analogs. *J. Raman Spectrosc.* **2019**, *50*, 1405–1415.
- (86) Wang, L.; Vendrell-Dones, M. O.; Deriu, C.; Doğruer, S.; de B. Harrington, P.; McCord, B. Multivariate Analysis Aided Surface Enhanced Raman Spectroscopy (MVA-SERS) Multiplex Quantitative Detection of Trace Fentanyl in Illicit Drug Mixtures Using a Handheld Raman Spectrometer. *Appl. Spectrosc.* **2021**, *75*, 1225–1236.

